Vibration Damping In Multispan Heat Exchanger Tubes

by

Timothy Dickinson

A thesis submitted in conformity with the requirements
for the degree of Master of Applied Science
Graduate Department of Mechanical Engineering
University of Toronto

Abstract

Good heat exchanger design requires that the designer understands and accounts for flow-induced vibration mechanisms. These mechanisms include vortex shedding, turbulent excitation and fluidelastic instability. Including the effects of these mechanisms in a vibration analysis of a heat exchanger requires information about damping. Multispan heat exchanger tube damping consists of three main components: viscous damping along the tube, friction and squeeze-film damping at the supports. Unlike viscous damping, squeeze-film damping is poorly understood and difficult to measure. In addition, the effect of temperature-dependent fluid viscosity on tube damping is not yet understood.

Experiments were done with two instrumented test rigs. Each rig contained a single vertical heat exchanger tube with multiple spans and a random excitation mechanism. Tests were conducted in air and in water at three different temperatures (25, 60 and 90°C). A new computer tool was developed to measure tube response to random excitation. This tool was also used to measure damping. Another new computer tool was developed to measure energy dissipation rates at the rig supports and the rate of energy used to excite the tube. The dissipation rate of input energy was also used to calculate damping. Results indicate that damping does not change over the range of temperatures tested. Results also show that measuring energy dissipation rate may be a useful way of estimating damping.

Dedication

This thesis is dedicated to my parents, David and Karen Dickinson, who inspired me to undertake higher levels of learning; and to my friends Dino Cule and Mark Biegler, who inspired me to complete those levels.

Acknowledgements

I acknowledge the invaluable efforts of Michel Pettigrew and Colette Taylor, of Atomic Energy of Canada Limited, and thank them wholeheartedly. Without them, this work could not have been initiated or accomplished.

I acknowledge the guidance of Professor Iain Currie, of the graduate department of Mechanical Engineering at the University of Toronto, and thank him for his supervision. His instruction, help, suggestions, experience, and patience were beyond the call of duty.

I acknowledge the assistance of Kerry Boucher and Murray Weckwerth, both formerly of Atomic Energy of Canada Limited, and thank them as well. Both helped me in concept and practice along the way.

I also acknowledge the resources—human, financial, and material—made available to me by Atomic Energy of Canada Limited and the Natural Sciences and Engineering Research Council and administered by Michel Pettigrew and Iain Currie. Without those resources, this work could not have been carried out.

Contents

List of Symbols and Acronyms

c_m	confinement effect
D	tube diameter [m]
D_e	tube bank effective diameter [m]
ℓ_m	characteristic span length [m]
f	tube vibration frequency [Hz]
f_n	natural frequency [Hz]
F	force [N]
L	support length parallel to tube [m]
m	mass per unit tube length [kg/m], or span mass [kg]
M(x)	mass function for tube and fluid [kg/m]
N	number of tube spans
ν	kinematic viscosity [m^2/s]
ϕ	phase [rad]
Φ	tube mode shape
ρ	density [kg/m^3]
S	Stokes number
t	time [s]
W	work [J]
W_d	tube energy dissipated at resonance [J/cycle]
x	displacement [m]

X	amplitude [m]
ζ	damping ratio [%]

A/D	analog to digital
CMRR	common mode rejection ratio
DAQ	data acquisition
DC	direct current
FFT	fast fourier transform
LabVIEW	laboratory virtual instrument engineering workbench
LSB	least significant bit
MB	megabytes
MTMDR	mid-temperature multispan damping rig
PC	personal computer
PIPO	heat exchanger vibration analysis program
RAM	random access memory
RMS	root mean square
RTMDR	room-temperature multispan damping rig
2PEAK	program to calculate damping via spectrum
VI	virtual instrument
VIVID	virtual instrument for vibration with integrated damping
VTU	Vibration and Tribology Unit
WAVEPAK	frequency analysis program
WAVI	work-rate analysis virtual instrument
WORMS	work rate measurement system

List of Tables

List of Figures

Chapter 1

Introduction

Nuclear reactors contain shell-and-tube heat exchangers. As their name indicates, these heat exchangers comprise a large outer shell housing many tubes. These tubes are supported at intervals along their length. These supports must be designed so that clearances around the tubes are sufficient for assembly and thermal expansion.

Thermal energy transfer occurs in heat exchangers by forcing a fluid through the tubes and another fluid (or fluid-gas mixture) across the tubes. This cross-flow induces tube vibration. If the vibration amplitudes are too large, damage or even failure can occur. Failure is due to mechanisms such as fatigue (progressive fractures at areas of high local stress caused by tube deflection) or fretting-wear (wear caused by relative motion between the tube and the support while in contact).

Large vibration amplitudes occur due to several phenomena such as vortex shedding, turbulent excitation, or fluidelastic instability. A flow-induced vibration analysis of a heat exchanger at the design stage must therefore include these phenomena. To do this, damping must be understood.

1.1 Problem

There are three main components of damping for multispan heat exchanger tubes in fluid: viscous damping along the tube length, friction and squeeze-film damping at the supports. Viscous tube-to-fluid damping is well understood and formulae for its calculation are available[1]. Friction and squeeze-film damping, however, are poorly understood and not so easily estimated.

1.1.1 Measuring Damping

Two known methods of measuring damping are the logarithmic-decrement method and the frequency response curve fit method[2]. A problem common to these methods is that they require time decay signals or vibration amplitude response peaks that can be reasonably approximated by ideal functions. Data that are not easily approximated by these functions do not yield reliable measurements of damping. Another method of measuring damping would be useful.

1.1.2 The Effect of Temperature on Damping

Heat exchangers often operate with two-phase water-steam mixtures at temperatures greater than 250 °C. However, much of the experimental damping work has been done at room temperature. Results from such experiments may not be adequate in all situations since damping depends on fluid viscosity, and viscosity varies with temperature. Information about how temperature affects damping would be useful.

[1] These formulae are discussed in Subsection 2.2.2.
[2] These methods are described in Section 2.3.

1.2 Approach

A heat exchanger tube vibrates due to the energy it receives from turbulent cross-flow and other vibration excitation mechanisms. The tube does not store any of the transferred energy, and so this energy must be dissipated through the available damping mechanisms. The rate of energy dissipation must be related to the amount of damping in the system. This thesis marks the first known time that this energy approach was used to estimate damping.

Chapter 2 reviews the theory and the published experimental results for the two main areas of interest: damping mechanisms of heat exchanger tubes and heat exchanger tube work-rates.

Chapter 3 describes the two experimental rigs used for this work. Concepts that governed the design of one rig are discussed. Data analysis methodology is also described.

Chapter 4 describes the three computer programs used to analyze the experimental data. Special attention is given to the two programs which were developed for this thesis.

Chapter 5 contains the results of the data collection and analysis with the programs described in Chapter 4.

Chapter 6 discusses the results of the data analysis.

Chapter 7 discusses what this study has accomplished.

The Appendices to this thesis contain information about the computer hardware and software utilized in this study.

Chapter 2

Literature Review and Theory

Two concepts require review. One is damping, or the energy dissipated by a system. The other is work-rate, or rate of mechanical energy transfer.

This chapter begins with a section that describes the types of motions observed for tubes within their supports. Following this are two sections: one on damping ratios and another on methods for measuring them. The chapter concludes with a section on work-rates. That section includes a proposal for estimating heat exchanger tube damping ratios using an energy balance approach.

2.1 Tube-Support Configurations

When heat exchangers are assembled, tubes are inserted into holes in baffle-plates or anti-vibration bars are placed between the tubes. Clearance between the tubes and their supports is necessary for assembly and maintenance. No special attempt is made to center tubes in their supports (centering is impossible in horizontal heat exchangers).

Most heat exchanger tube vibration analysis programs simplify calculations by assuming that there is always a solid contact between a tube and its support (i.e., a circumferentially pinned support condition). In practice, several different tube-support configurations may exist:

- *Centered*, when the tube and the support are perfectly aligned along the support length (nearly impossible to achieve).
- *Eccentric*, when the tube is closer to one side of the support than the other.
- *Impacting*, when the tube rests touching the inside support surface and frequently impacts on the support when it vibrates. A variation of impacting is *contacting*, when a tube touches the support but does not "lift off" from the surface.
- *Sliding*, when the tube slides around the inside support surface.
- *Scuffing*, when the tube simultaneously impacts and slides on the inside support surface.

Real tube-support interaction is a complex—and often random—combination of these configurations. These configurations are illustrated in Figure 2.1.

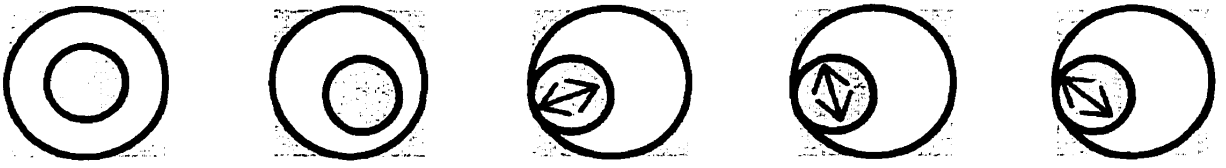

Figure 2.1: Tube/Support Configurations

When a tube impacts, slides, or scuffs in a support (i.e., there is significant contact) that support is said to be *effective*. An effective support is one that acts like a pinned support. When a tube is centered or eccentric in a support and vibration amplitudes are small the tube may contact the support infrequently or not at all. In this case, the support condition is said to be *ineffective*. Ineffectively supported tubes no longer behave as though all spans are pinned at each end. Analyses that assume they are effectively pinned will be in error.

2.2 Damping

There are different ways of expressing the amount of damping, or rate of energy dissipation, in a system. When damping is quantified, this thesis will use the *damping ratio* which is the ratio of the actual damping coefficient to the critical damping coefficient of a system.

2.2.1 Energy Dissipation Mechanisms

The annular gaps between heat exchanger tubes and their supports are too large to model the tube-support interaction with lubrication theory (which neglects fluid inertia) and too small to allow ideal flow modeling (which neglects fluid viscosity). It is therefore necessary to understand the forces and effective mass and damping associated with the fluid-filled annular gaps. Mulcahy [1] derived approximate expressions for the fluid forces, lumped added-mass, and linear damping of tubes in annular regions such as a drilled-hole support. Mulcahy used these approximations to predict the fundamental frequency and damping of a single beam for the following conditions:

- small fluid motions
- finite-length open-ended annular regions
- gap-to-radius ratio $\ll 1.0$
- viscous penetration of the order of gap width

Rogers et al. [2] reviewed this and other literature for heat exchanger tube-fluid effects. This review included effects that occur along the tube and effects that occur within the clearance between each tube and support. After developing models for added-mass and fluid damping, Rogers et al. concluded that the added-mass formula by Mulcahy is acceptable. They also found that more accuracy is required to properly model squeeze-

film damping for all except very small tube motions. Both the Mulcahy and Warner-Sommerfeld [3] models are reliable for very small motions.

To improve that damping model, Pettigrew et al. [4] outlined several damping mechanisms that occur in heat exchanger tube-support interactions. Those mechanisms are listed in Table 2.1.

Table 2.1: Heat Exchanger Tube Damping Mechanisms

Type of Damping	Source
Structural	Internal to tube material
Viscous	Between fluid forces and forces transferred to tube
Flow-dependent	Varies with flow velocity
Squeeze-film	Between tube and fluid as it approaches support
Friction	Coulomb damping at support
Two-phase	Due to liquid/gas mixture

Damping In Gases

After a review of existing experimental results Pettigrew et al. [5] created guidelines for the design of heat exchanger tubes in gases. Pettigrew et al. concluded that friction damping was the most significant type of damping in gases. Therefore the number of supports and support length are the most important damping parameters in gases. Diametral clearance between tube and support is far less important. Parameters such as frequency, mass, and diameter appear to have no dominant effect on damping in gas.

Damping In Liquids

Pettigrew et al. [6] also made recommendations for the design of heat exchanger tubes in liquids. A large amount of damping data from various sources were considered. The

result was a conservative minimum damping ratio criterion. That criterion is based on the three main dissipation mechanisms:

- In a still fluid the tube-to-fluid *viscous damping* is related to the Stokes Number (defined in Equation 2.4) and to the degree of tube confinement within a tube bundle (i.e., the proximity of other tubes).

- *Squeeze-film damping* appears to be the dominant damping mechanism in liquids. It occurs due to fluid forces generated in the annular clearance between the tube and its supports as the tube motion squeezes the fluid against the support.

- *Friction damping* is more difficult to quantify than the first two. For typical tubes, contact often does occur. However, it becomes difficult to separate friction damping effects from squeeze-film damping. Pettigrew et al. left friction damping as part of squeeze-film damping.

Experimental Programs

Pike and Taylor [7] carried out an experimental program to study damping of multispan steam generator tubes.

For preloaded tubes, damping ratio values obtained by the logarithmic-decrement and frequency response curve fit method were similar[1]. Damping ratios measured at each of the three midspan locations were consistent. The damping ratios tended to increase with increased excitation.

For tubes centered in their supports, frequency and damping measurements were very different between the two methods. Pike and Taylor decided that the support conditions must have been different between the preloaded tests and the centered tests. Damping ratios measured at each of the three midspan locations varied significantly.

[1]Both methods are explained in greater detail in Section 2.3.

2.2.2 Current Design Recommendations

Pettigrew et al.'s identification of tube damping mechanisms include formulae for the significant sources of damping in heat exchanger tubes. These formulae are given in the following subsections. Note that the viscous damping ratio formula is an exact theoretical relation. Formulae for friction and squeeze-film damping are semi-empirical and generally define a minimum (i.e., worst-case) level of damping for design purposes.

Friction Damping

According to Pettigrew et al. [5], [6], the friction damping ratio (expressed in percent) of a multispan tube is

$$\zeta_{f,gas} = 5.0\left(\frac{N-1}{N}\right)\left(\frac{L}{\ell_m}\right)^{\frac{1}{2}} \tag{2.1}$$

$$\zeta_{f,liquid} = 0.5\left(\frac{N-1}{N}\right)\left(\frac{L}{\ell_m}\right)^{\frac{1}{2}} \tag{2.2}$$

where N is the number of tube spans, L is the support length, and ℓ is the *characteristic span length.* Characteristic span length is defined to be the average of the three longest spans of a multispan tube in cross-flow. The characteristic length is defined this way because the vibration amplitudes of the longest spans will be largest at the lower (and most commonly seen) modes.

Viscous Damping

Rogers' simplified version of the cylinder viscous damping theory of Chen et al. [8] gives the damping ratio (in percent) of a tube vibrating in a liquid as

$$\zeta_v = \frac{100\pi}{\sqrt{8}}\left(\frac{\rho D^2}{m}\right)\left(\frac{2\nu}{\pi f D^2}\right)^{\frac{1}{2}}\left\{\frac{1+\left(\frac{D}{D_e}\right)^3}{\left[1-\left(\frac{D}{D_e}\right)^2\right]^2}\right\} \tag{2.3}$$

where ρ is the fluid density, m is the mass per unit tube length, including the mass of the interior fluid and hydrodynamic mass, D_e is the effective diameter of the surrounding

tubes, D is the tube diameter, ν is the fluid kinematic viscosity, and f is the frequency of tube vibration.

This equation is valid when the Stokes number is greater than 3300 and the ratio $\frac{D}{D_e}$ is less than 0.5. The Stokes Number, S, is defined as:

$$S = \frac{\pi f D^2}{2\nu} \tag{2.4}$$

Squeeze-Film Damping

According to Pettigrew et al. [6], the squeeze-film damping ratio (in percent) for a multispan tube in a liquid is

$$\zeta_{sf} = \left(\frac{N-1}{N}\right)\left(\frac{1460}{f}\right)\left(\frac{\rho D^2}{m}\right)\left(\frac{L}{\ell_m}\right)^{\frac{1}{2}} \tag{2.5}$$

Equation 2.5 is not dimensionless, due to the term $\frac{1460}{f}$. This equation is not a theoretical derivation for squeeze-film damping. It is an empirical expression that describes the lower bound of a set of experimental data.

2.3 Damping Ratio Calculation Methods

There are two well-known methods for measuring damping. The *logarithmic-decrement* (log-dec) method uses the logarithm of the ratio of different oscillation amplitudes of a decaying free vibration. A greater log-dec value indicates greater damping. The *frequency response* method uses a curve fit of an amplitude frequency response spectrum of the system. One of the parameters of the function that fits the curve is the damping ratio.

Both of the above methods work well when the system being analyzed has only one degree of freedom and, therefore, only one distinct natural frequency (or, at least, only one distinct frequency within a fairly broad frequency band). This is not always the case, however. The amplitude spectrum may contain two or more peaks very close together. This can occur when a vibrating tube impacts at different locations in a support of non-zero length. The result is slightly changing vibration modes and two or more spectral

peaks. Multiple peaks can also occur when the material properties of a system are slightly different in one direction than in another.

The experiments done for this work used real tubes of typical materials and supports. Adjacent spectral peaks did occur. Only one of the above methods of damping ratio calculation can be made to account for two peaks: curve-fitting the frequency response spectrum.

2.3.1 Curve Fitting

A best-fit characteristic equation can be applied to experimental amplitude spectrum data. The parameters of the resultant fitted equation are the natural frequency, the static deflection (also called the zero-frequency amplitude), and the damping ratio. If there is only one spectral peak, a linear least-squares numerical regression method will provide the parameters. If there are two peaks, a non-linear least-squares method must be used.

2.3.2 The Marquardt Method

Data is often categorized by fitting it to a model of adjustable parameters. The model may be some convenient function or may be constrained by a suspected underlying theory.

In most cases this is done by using a *merit function* that measures the agreement between the data and the model with a particular set of parameters. If the merit function is arranged so that small values represent good agreement—as is usually the case—the model parameters are adjusted to minimize the merit function. Parameters that achieve the minimum merit function (or that decrease the merit function to an acceptable level) are called the *best-fit parameters.*

Methods for solving a linear least-squares problem are well-documented. The problem here is curve-fitting two adjacent peaks in a frequency response function. A non-linear method must be used to solve for all the parameters.

Mastorakos [9] outlined a procedure using a least-squares estimation of non-linear parameters developed by Marquardt [10].

When the model depends nonlinearly on a set of M unknown parameters a_k, $k = 1, 2, \ldots, M$, the same merit function-minimization approach is used as for the linear case. The minimization must be done iteratively by improving parameter values until the merit function effectively stops decreasing.

The Marquardt method is generally accepted as an elegant, robust, non-linear regression model. It has become the standard in non-linear least-squares routines [11]. It is used here to fit the frequency response spectra functions of the midspan amplitude data.

The data can be fitted by an equation of the form:

$$g = g\left(x_1, x_2, \ldots, x_m, P_1, P_2, \ldots, P_p\right) \tag{2.6}$$

where x are independent variables and P are constant parameters of the function. A satisfactory solution is found by determining the best estimates, P_m, of the parameters, P, to minimize the following equation:

$$\text{Residual} = \sum_{i=1}^{n} \left(Y_i - Y_i^A\right)^2$$

Here, Y_i are dependent variables, Y_i^A are the amplitudes calculated from Equation 2.6, and n is the total number of data points. Marquardt's procedure determines corrections to apply to the estimated parameters P_m at each iteration by solving the following equation:

$$\left([Z]^T [Z] + \lambda [I]\right) [S] = [Z]^T \left(Y_i - Y_i^A\right)$$

In this,

$$[Z] = \begin{bmatrix} \frac{\partial g(Y_1)}{\partial P_1} & \frac{\partial g(Y_1)}{\partial P_2} & \cdots & \frac{\partial g(Y_1)}{\partial P_p} \\ \frac{\partial g(Y_2)}{\partial P_1} & \frac{\partial g(Y_2)}{\partial P_2} & \cdots & \frac{\partial g(Y_2)}{\partial P_p} \\ \vdots & \vdots & \ddots & \vdots \\ \frac{\partial g(Y_n)}{\partial P_1} & \frac{\partial g(Y_n)}{\partial P_2} & \cdots & \frac{\partial g(Y_n)}{\partial P_p} \end{bmatrix}$$

where $[S]$ is a vector of small corrections applied to each parameter, $[I]$ is the identity matrix, p is the number of parameters, and λ is a convergence parameter.

Initially, the user must supply guesses for each parameter. The method calculates corrected estimates after each iteration, k, through the equation:

$$p_m^{k+1} = p_m^k + s_m^k$$

An iteration is complete when

$$\frac{|S_j|}{0.0001 + |P_{mj}|} < \epsilon$$

where ϵ is an arbitrary convergence criterion.

2.3.3 Application to Two-Peak Damping Ratios

To measure the damping ratio parameter using the Marquardt method, the frequency response function that describes the amplitude spectrum is required.

For one spectral peak the function is:

$$\begin{aligned} Y(f) &= \frac{X}{X_0} \\ Y(f) &= \frac{1}{\sqrt{\left[1 - \left(\frac{f}{f_n}\right)^2\right]^2 + \left[2\zeta\left(\frac{f}{f_n}\right)\right]^2}} \end{aligned}$$

For two adjacent peaks:

$$g = Y_1(f) + Y_2(f)$$

where X_0 is the amplitude at $f = 0$ (the static deflection), f_n is the natural frequency and ζ is the damping ratio.

Each of these cases has only one independent variable: f. For one peak there are three parameters: $Y_{0,1}$, f_{n1}, and ζ_1. For two peaks there are six parameters: $Y_{0,1}$, f_{n1}, ζ_1, $Y_{0,2}$, f_{n2} and ζ_2.

In the one-peak case, the equation can be rearranged to isolate each parameter to obtain the solution. This is not possible in the two-peak case, and so the Marquardt method is used.

2.3.4 Difficulties with these Methods

The aforementioned methods—log-dec and curve-fitting peaks on a frequency response plot—are accurate when the time or frequency signal to be analyzed is distinct. That is, if a tube vibrates only (or mainly) at one frequency, these methods work well. It has also been shown that the frequency response curve-fit method can be extended to two adjacent peaks (representing a tube that is vibrating at two close frequencies).

Both methods lose accuracy, however, when the support conditions and the vibration modes become more dynamic. Tube/support interaction can produce very non-linear behaviour that is characterized by a "cluster" of close frequencies. In a frequency response function these appear as a very broad single peak. A damping ratio calculated from a fit of this broad peak would not be accurate.

This was a reason for considering an energy approach. Balancing the total energy dissipated by tube motion does not require an understanding of how the support conditions change. If the approach proves successful, the difficulties of dealing with non-linearities will be greatly reduced.

2.4 Work-Rates

Work-rate denotes a mechanical energy exchange that takes place at a particular average rate. The quantity is therefore more properly defined as *power*. However, the term work-rate has been commonly used in the fretting-wear study of heat exchanger tubes. The term is used here as well.

In fretting-wear studies, work-rate is defined as the rate of energy dissipation as a

tube in contact with its support moves circumferentially [12]. This relation is described by the equation

$$\frac{dW}{dt} = \frac{1}{t}\int F\,ds$$

where W is the work-rate, t is time, F is the normal contact force, and s is the sliding distance. A force (the contact force between tube and support) multiplied by a displacement (as the tube slides) results in work. Although these vectors are orthogonal, fretting-wear studies have shown that the material damage rate is closely related to the normal forces during contact.

Pike and Taylor attempted to measure work-rates in their experiments[2]. Tube-support impacts were of insufficient magnitude to measure work-rates, however. Pike and Taylor concluded that for the tests where the tube was centered the tube never achieved large enough motions. For their preloaded tests they concluded that the tube never received sufficient excitation levels to lift off from the support.

2.4.1 Work-Rates as Damping Ratio Estimators

Damping is a measure of the rate of energy transfer. Relating work-rate to damping seems reasonable. This might result in another method of estimating the damping if two equations are met:

1. reliable work-rate measurements that can be associated with the rate of energy loss of a system can be made, and

2. the damping measured with a work-rate method agrees with that estimated with known methods.

It is assumed that a multispan tube can be simplified to three single-span simply-supported tubes. For a simple one-degree-of-freedom system comprising a spring, mass,

[2]See Subsection 2.2.1.

and viscous damping, the harmonic displacement and velocity are defined as follows:

$$\begin{aligned} x &= X \sin(2\pi f t - \phi) \\ \frac{\mathrm{d}x}{\mathrm{d}t} &= 2\pi f X \cos(2\pi f t - \phi) \end{aligned}$$

According to Thomson [13], the energy dissipated per cycle of vibration at resonance, W_d, for this system is

$$W_d = 8\pi^3 m \zeta {f_n}^2 X^2 \tag{2.7}$$

where m is the equivalent mass, ζ is the damping ratio, f_n is the natural frequency, and X is the peak amplitude of vibration.

From Equation 2.7, the equivalent viscous damping is estimated by

$$\zeta = \frac{W_d}{8\pi^3 m f_n^2 X^2} \tag{2.8}$$

The equivalent mass for the tube is calculated from

$$m = \int_{\text{tube length}} M(x)\Phi^2(x)\,\mathrm{d}x \tag{2.9}$$

where $M(x)$ is the mass of the tube plus the added interior water and hydrodynamic mass per unit length of tube, and $\Phi(x)$ is the mode shape of the tube. If the tube mode shape is being approximated by a sinusoidal function then $\Phi(x) = \sin(\pi x/\ell)$. In this equation, x is the vertical location along the span, and ℓ is the length of the span.

Calculating the energy dissipated in this way requires the peak vibration amplitudes. The excitation of heat exchanger tubes by turbulence is random. The peak amplitude of a zero-mean random signal may be assumed to be three times the standard deviation (equivalent to the RMS) value, since approximately 99.7% of the random amplitudes will fall within that limit. Equation 2.8 is for sinusoidal vibration, however—a peak amplitude for this motion would be $\sqrt{2}$ times the RMS value. As an approximation, and since rig components surrounding the tube may constrain vibration, a peak amplitude of vibration of twice the RMS value will be assumed.

Knowing the shaker power transferred to the tube, and assuming a one-degree-of-freedom vibration, an equivalent damping ratio can be calculated. In this case the assumed amplitude of vibration is the average amplitude of the three spans. The effective mass is the sum of the mass of the three spans.

It bears repeating that, at the time of this work, this energy approach to estimating damping had not been attempted. It is also worthwhile to note that since this work was completed more use has been made of this method. Results published by Taylor et al. [14] used the equipment and analysis programs developed for this study to test heat exchanger tubes under different support pre-load conditions. These results, and the energy method for estimating damping that was used, were reviewed by Pettigrew et al [15]. They were also used by Yetisir et al. [16] in the development of an operational heat-exchanger specification based on work-rate.

Chapter 3

Experimental Procedure

Two sets of experiments were completed for this work. The first set is from the original room-temperature multispan damping rig and is discussed in Section 3.1. These experiments provide results that act as a baseline for the design and evaluation of a higher-temperature rig. The second set of experiments are from the newly-constructed mid-temperature multispan damping rig. These experiments are discussed in Section 3.2. These experiments provide more data points in the investigation of the effect of temperature on damping. These data may serve as an indicator of whether further high-temperature damping experimentation is necessary.

3.1 Room-Temperature Multispan Damping Rig (RTMDR)

The Room-Temperature Multispan Damping Rig (RTMDR) was constructed several years before this testing was begun. It was used for many sets of experiments in the Vibration and Tribology Unit (VTU) of Atomic Energy of Canada Limited. In that time, the RTMDR underwent significant adaptations and evolutions.

3.1.1 Construction and Instrumentation

The RTMDR is essentially a heat exchanger tube in a stainless steel trough. The rig—originally used horizontally—stands vertically to an overall height of about 4 m. The trough has three sides. The front is opened and shut with a swinging door lid. The trough is open to the atmosphere at the top. A picture of the RTMDR is shown in Figure 3.1.

Inside the RTMDR trough are two long vertical plates attached to the back of the trough. These plates are supported at intervals with fins and bars that attach to the trough sides. Midspan and support platforms fasten to these two vertical plates. The platforms may be moved and fixed at any location along the tube. Changing the support platform locations changes the lengths of the tube spans.

The RTMDR heat exchanger tube properties are shown in Table 3.1. Each RTMDR tube span length is 1.219 m.

Table 3.1: Heat Exchanger Tube Properties

Material	Incoloy 800
Inner diameter	13.7 mm
Outer diameter	15.9 mm
Free length	3.74 m
Density	7.944 kg/m^3
Modulus of elasticity	1.97×10^{11} N/m^2

There are six platforms along the tube at even intervals. Each platform has transducer assemblies. Three platforms have brass drilled-hole supports (see Figure 3.2). Support platforms are instrumented with two eddy-current displacement probes—aimed at a target ring on the tube and positioned 90° apart—and a ring with four piezoelectric force transducers. The force transducer ring is in contact with the support. Any contact force

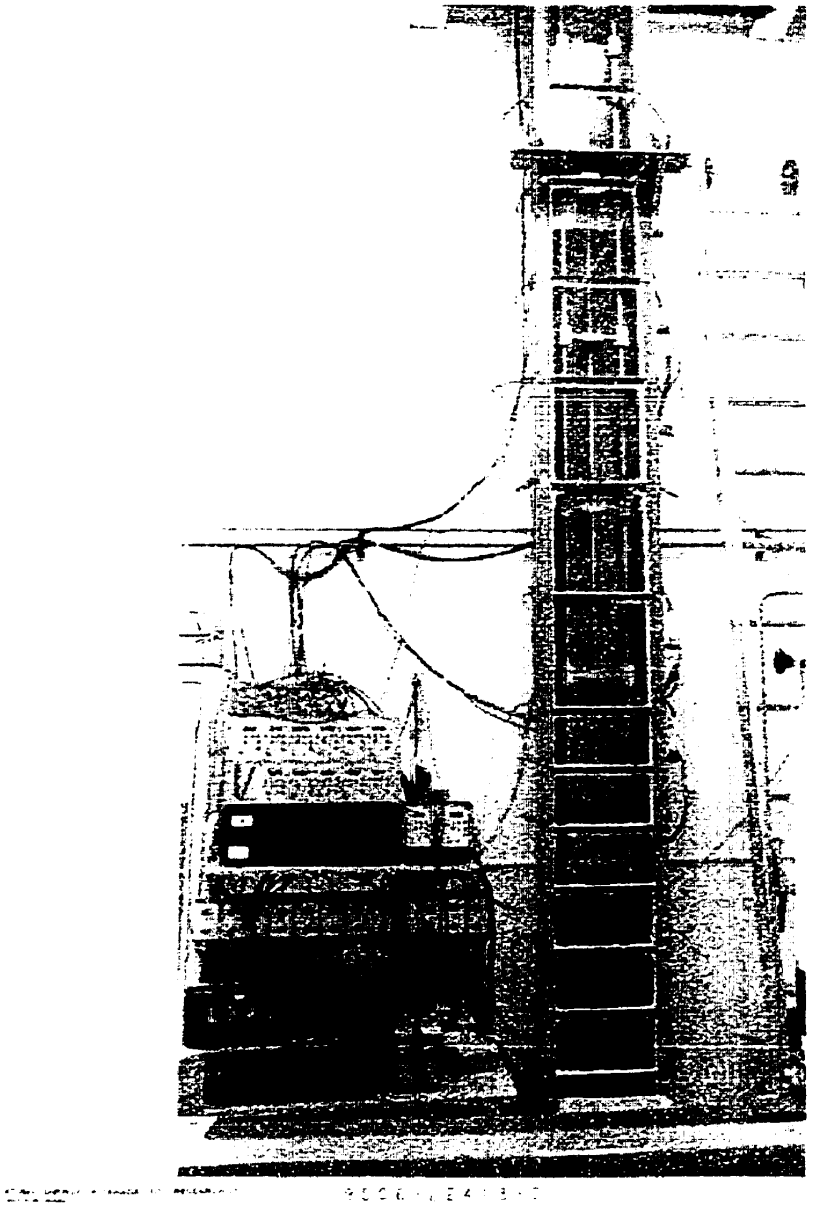

Figure 3.1: RTMDR Experimental Setup. The front face of the trough rig (right) is a Plexiglas lid. The tube can be seen in the centre of the trough as can several of the support and midspan transducer platforms. The shaker platform is near the top of the trough (shakers not shown). Sensor signal wires leave through the right side of the trough. Excitation, measurement, and recording instruments are shown (left).

between the tube and the support results in a signal from the force transducers.

By using four force transducers the direction of impact can be determined. Piezoelectric force sensors only produce positive signals. They emit a charge only when they are compressed. Opposite-direction force signals at each support are added via summing boxes. This produces two orthogonal force measurements at each support. See Figure C.1 for a force ring arrangement diagram.

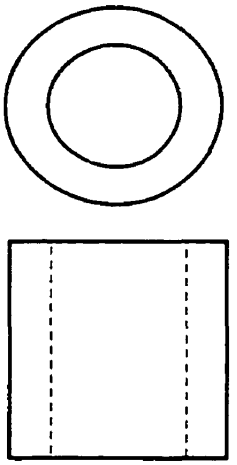

Figure 3.2: RTMDR Brass Drilled-Hole Support

Three platforms do not have supports. They have large holes that do not interfere with tube movement and are for transducer placement at the midspans only. The arrangement of support and midspan platforms is shown in Figures 3.3 and 3.4, respectively.

Two vibration generators (shakers) excite the tube. The shakers are clamped to a steel platform that is bolted to the trough lid. The input motion signals are supplied by two random noise generators. These signals are filtered to bandpass frequencies between 1 and 100 Hz.

The shakers connect to the tube through a series of attachments. Figure 3.5 shows a picture of the shaker and assembled attachments. Figure 3.6 shows the same equipment when disassembled. A threaded rod on the shaker (A) connects to an impedance head (B). A short rod (C) and a collar (D) with two set-screws provide length adjustability

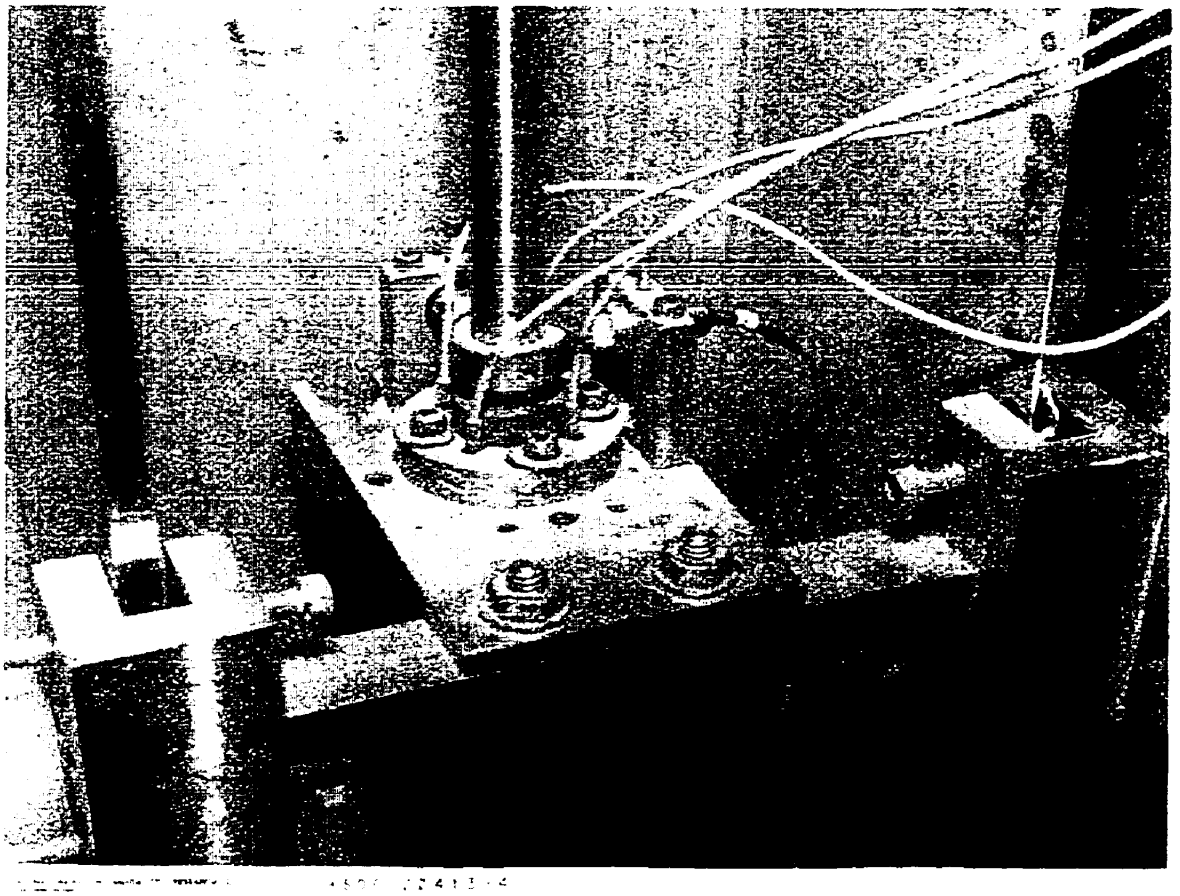

Figure 3.3: RTMDR Support Arrangement. The brass tube support is surrounded by the force ring (four wires leading upwards show the locations of the piezoelectric force transducers in the ring). The support and ring sit on the support platform. The platform is laterally adjusted and held in place by set screws in the arms that fit over two vertical plates in the trough. Just above the support is a target ring on which the two eddy-current proximity probes (90° apart, wires hanging downward) take displacement measurements.

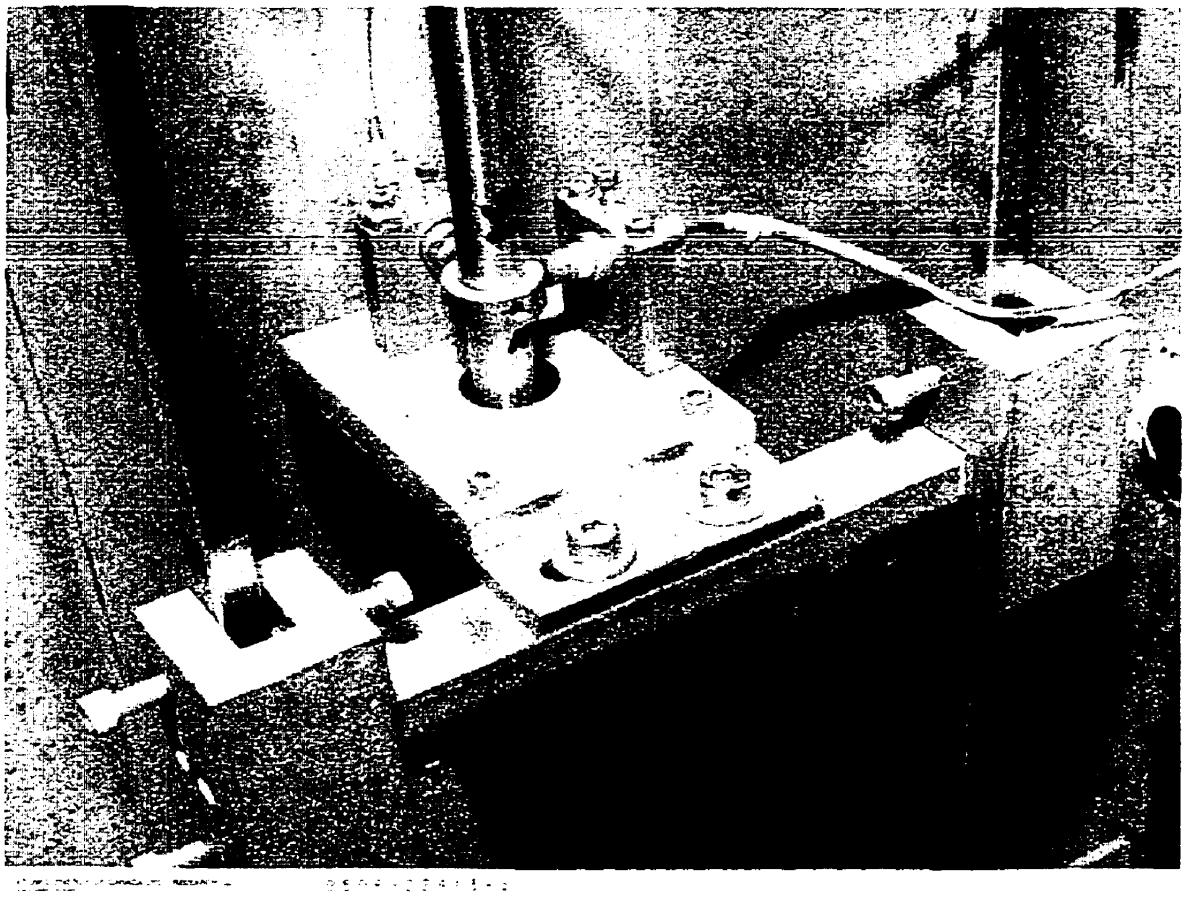

Figure 3.4: RTMDR Midspan Arrangement. The tube passes through a hole in the platform. This hole is sized large enough so that the vibrating tube will not contact it. The platform is laterally adjusted and held in place by set screws in the arms that fit over two vertical plates in the trough. There is a target ring at this location on which the two eddy-current proximity probes (seen 90° apart) take displacement measurements.

to facilitate installation. The collar fastens to a threaded rod (E) that attaches to a short section of steel cable with threaded brass ends (F). The cable is needed to align the shaker rods with the pass-throughs and tube connection. The cable connects to a brass collar that tightly encircles the tube. Shaker attachment through the front lid door to the tube is shown in Figure 3.7.

All test signals were recorded on a VHS cassette magnetic tape recorder.

3.1.2 Operation

The first step was to adjust the support platforms to center the tube in all three of its supports. This proved impossible since the tube—clamped at the bottom and free at all supports—is a thin, 3.74 m vertically cantilevered beam. Tube deflection always caused

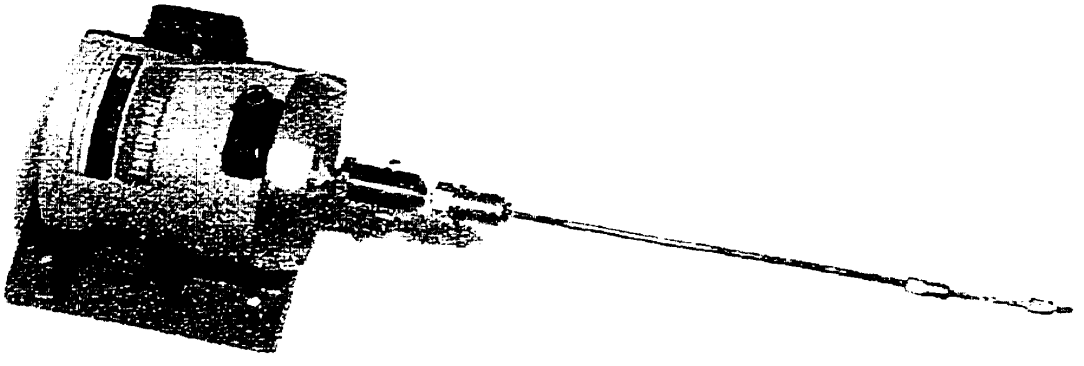

Figure 3.5: Shaker and Attachments (Assembled)

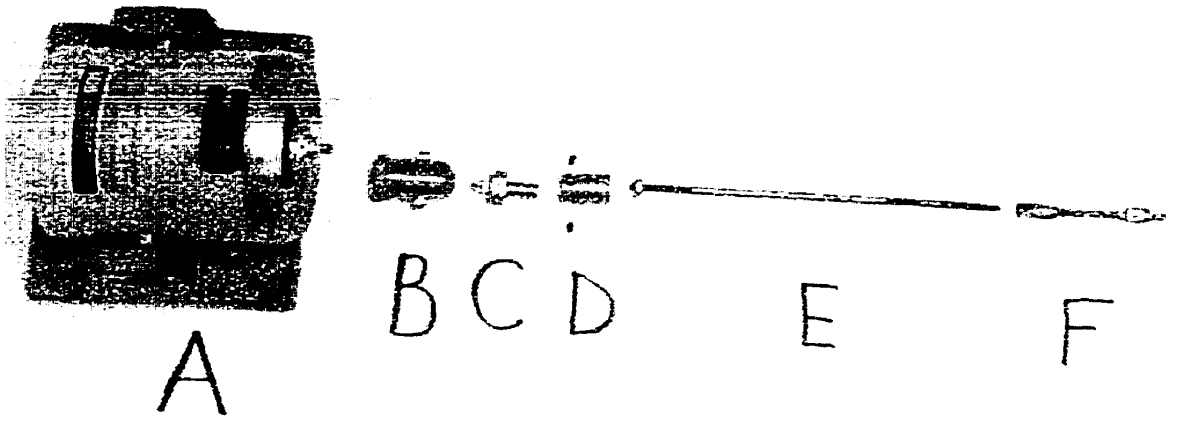

Figure 3.6: Shaker and Attachments (Disassembled)

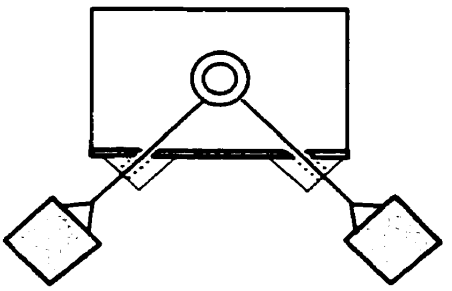

Figure 3.7: RTMDR Shaker Pass-Through Connections

contact with the top support. In the end, RTMDR testing was done with only the bottom support centered.

The next step was to check that all force and displacement sensors were operating properly. This was done before the front lid of the rig was closed, since closure prevents access to the trough interior. Once the front lid was closed (and all sealing clamps engaged for the water tests), the shaker rods were inserted through the pass-throughs and screwed into the tube collar. The shakers were positioned so that their rods moved freely through the pass-throughs. The shakers were then clamped down. Rubber diaphragms were fastened over the pass-throughs and attached to the shaker rods, if water tests were performed. For water tests, an attached water line valve was opened. This filled the trough.

The final step was to set the shaker power level. Signals were recorded to tape while the tube vibrated for several minutes.

RMS shaker forces for these tests are shown in Tables 3.2 and 3.3.

Table 3.2: RTMDR Air Test Excitation Levels

Test Level	Shaker RMS Force Input Level (N)
1	1.1
2	1.5
3	2.2
4	3.4

Table 3.3: RTMDR Water Test Excitation Levels

Test Level	Shaker RMS Force Input Level (N)
1	2.0
2	3.2
3	4.9

3.2 Mid-Temperature Multispan Damping Rig (MTMDR)

Testing in heated water would require substantial structural changes to the RTMDR. A new experimental rig—the Mid-Temperature Multispan Damping Rig (MTMDR)—was a more effective option.

There were three guidelines for MTMDR design:

1. *Operation must be safe.* The multispan damping rig is a tall container of heated water. There must be human operators present during testing. The rig must be located in an area where other equipment, experiments, and people operate. An operator must be satisfied that there will not be any water spillage.

2. *Keep as much original room-temperature rig design as is practical.* One reason for this is that the original RTMDR design has proven to be a simple and workable one. It was used for many experiments and was adaptable. Another reason is that the MTMDR can serve as a "stepping-stone" between measurements taken from the RTMDR and possible future high-temperature multispan damping experiments. Another reason is that a similar design may allow parts of the RTMDR to be used in the MTMDR. This minimizes cost and time.

3. *There must be a way to heat the water inside the rig.* To investigate the effect of

temperature on damping it must be possible to efficiently, safely, and accurately heat the water inside the rig.

3.2.1 Construction and Instrumentation

The MTMDR is—like the RTMDR—a single vertical heat exchanger tube clamped at the bottom and supported at three other equally-spaced locations. The entire rig may be enclosed so that the tube can be surrounded by water. Two back-to-back vertical C-shaped channels (see Figure 3.8) provide a frame for the transducer platforms. These channels and the tube clamp bolt to a heavy steel base plate on the floor. An overall view of the MTMDR is shown in Figure 3.9.

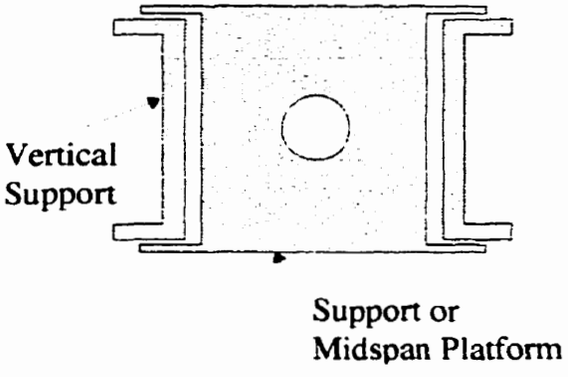

Figure 3.8: Top View of MTMDR Support Structure

The shell enclosing the rig is a stainless steel pipe. It has a bottom flange that is sealed by an O-ring in the floor baseplate. The shell has several electric heaters attached to its outside surface, so that water inside the shell can be heated. A layer of insulation covers the shell and heaters. The shell also has two holes at the top so that a crane may attach for shell installation and removal. The top of the shell is open to air to permit tube coupling to the shakers and to provide an easy exit for sensor cables. An open top also ensures that the inside rig test area cannot become pressurized if water evaporation occurs.

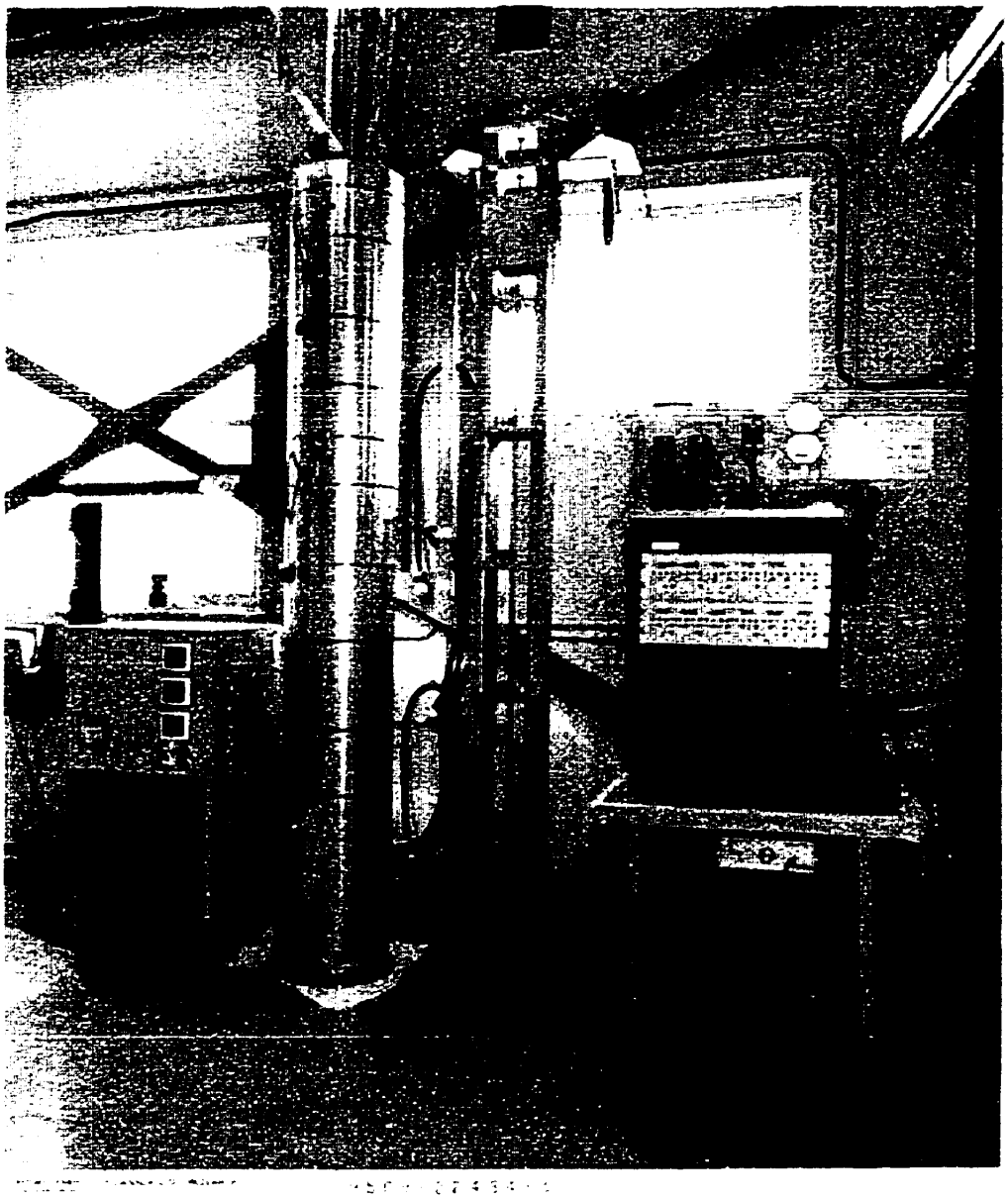

Figure 3.9: MTMDR Overall View. The heat exchanger tube is housed within the vertical channels (center). Evenly-spaced support and midspan platforms attach to the channels. Shakers (top) attach to the tube. The rig shell (left) is fitted with heaters and insulation (the heater plugs extend from the shell); the heater control unit can also be seen (far left). A table beside the rig (right) supports all instrumentation.

MTMDR support and midspan platforms are shown in Figures 3.10 and 3.11 respectively.

The shakers are bolted to a steel plate that is solidly attached to an adjacent interior wall. The shaker heads attach to a collar at the top of the tube (the tube extends several inches above the top of the shell). Figure 3.12 shows the shakers and how they attach to the MTMDR tube.

The MTMDR was developed to allow testing in water at higher temperatures. This was accomplished by attaching five 2500 W electric band heaters to the outside of the shell that encloses the rig. Figure 3.13 shows the positions of the heaters. Two heaters are located at the bottom of the shell. This concentrates heat input at the bottom of the water column when the liquid is initially heated. This warmer water will rise because of natural convection. The other three heaters are each located at shell positions corresponding to tube support locations.

All five heaters are wired to a control unit located beside the rig (see Figure 3.9). The two bottom heaters operate only by on/off switching and are generally used only to heat the water column to the target temperature. The other three heater temperature levels are set by manual analog dials on the control unit. Heaters are controlled by feedback from thermocouples attached to the rig near each heater.

The temperature control system also has a safety feature that prevents heater burnout in the case of water evaporation. A master control is wired to a safety thermocouple that is attached to the interior surface of the shell near the top heater. If the heaters are inadvertently left at a setting high enough to cause water evaporation, the liquid water level could drop enough over time to expose the inside shell surface to air. This would cause a jump in shell temperature and burnout damage to the shell, heater, or instrumentation. The master control will shut off all heaters if it registers a safety thermocouple temperature greater than 100 °C (indicating that all liquid water has evaporated down to that level).

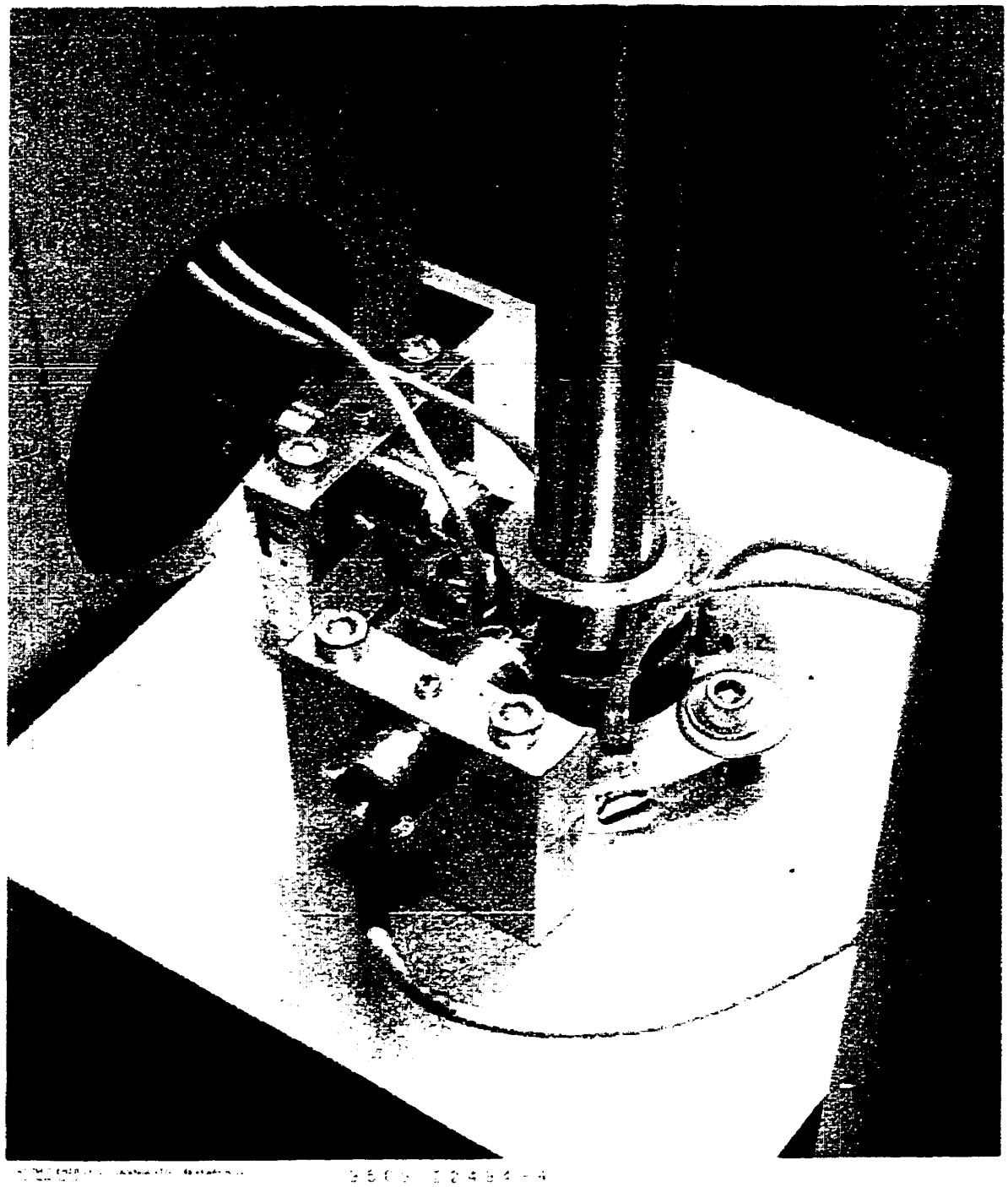

Figure 3.10: MTMDR Support Arrangement. The support arrangement is similar to the RTMDR (see Figure 3.3). The support is surrounded by a force ring with four force sensors. Two motion sensors measure displacement of a target ring.

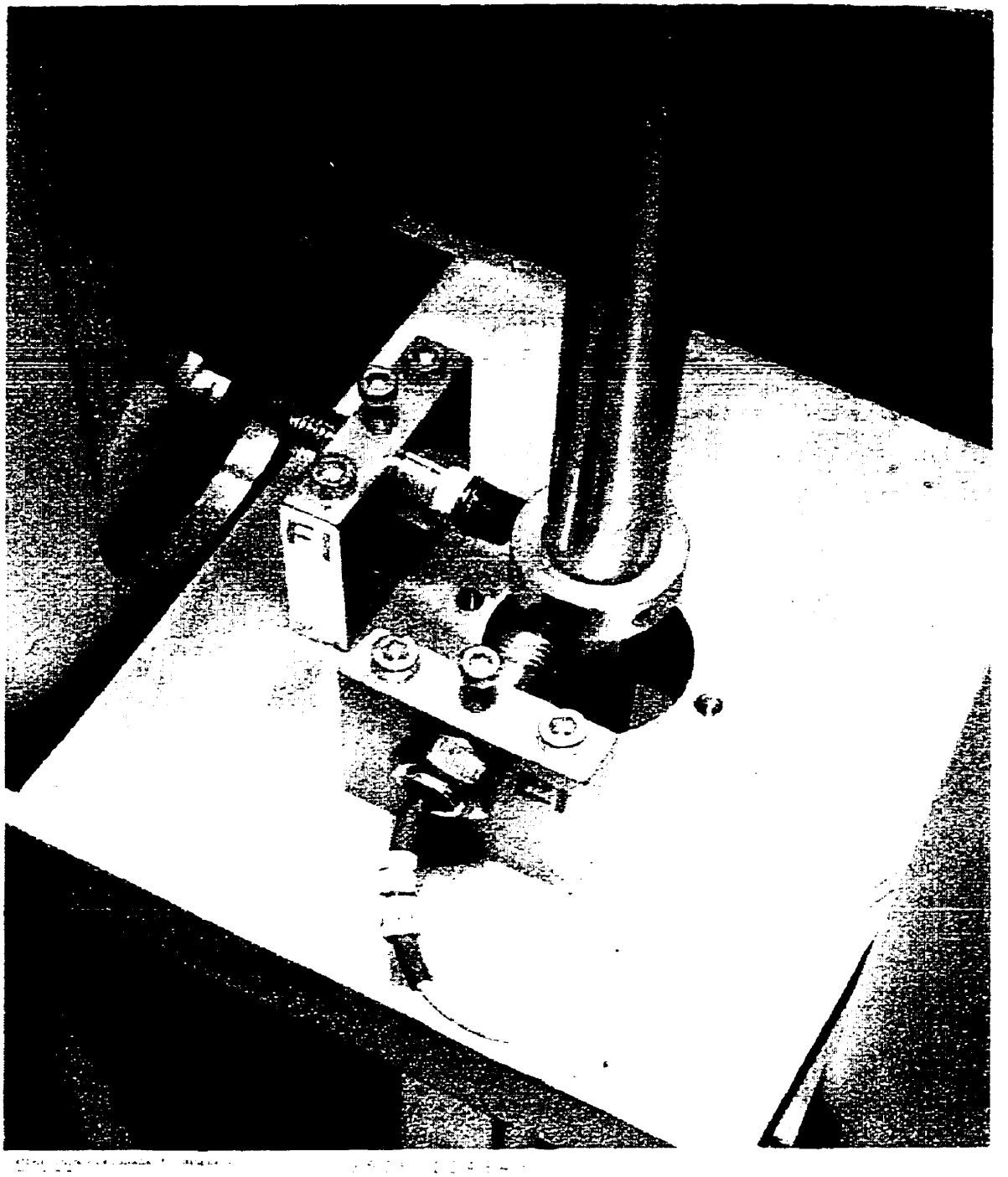

Figure 3.11: MTMDR Midspan Arrangement. The midspan platform arrangement is similar to the RTMDR (see Figure 3.4). Two motion sensors measure displacement of a target ring.

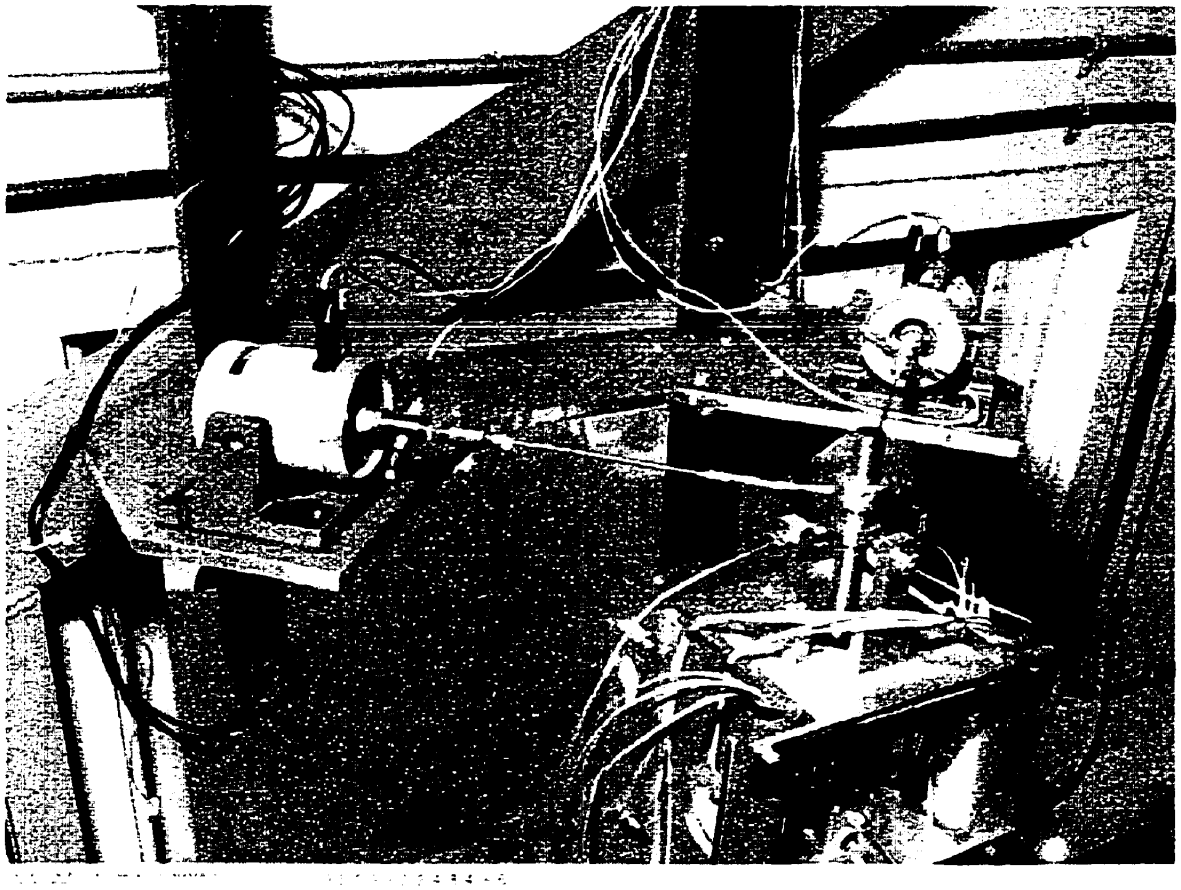

Figure 3.12: MTMDR Shaker Attachment. The shakers attach to a tube collar through a series of connectors (see Figures 3.5 and 3.6). Two motion sensors (90° apart) on the top of the rig measure the displacement of the tube just beneath the attachment point. Shakers receive their input signals via terminals on top of the shaker cylinder. Shaker force signals and acceleration signals (not used) are measured via outputs on the shaker impedance head. The shakers are bolted to their platform. The platform is attached to two vertical supports that are solidly bolted to the wall of the building that houses the MTMDR. Thermocouple leads can also be seen (far left).

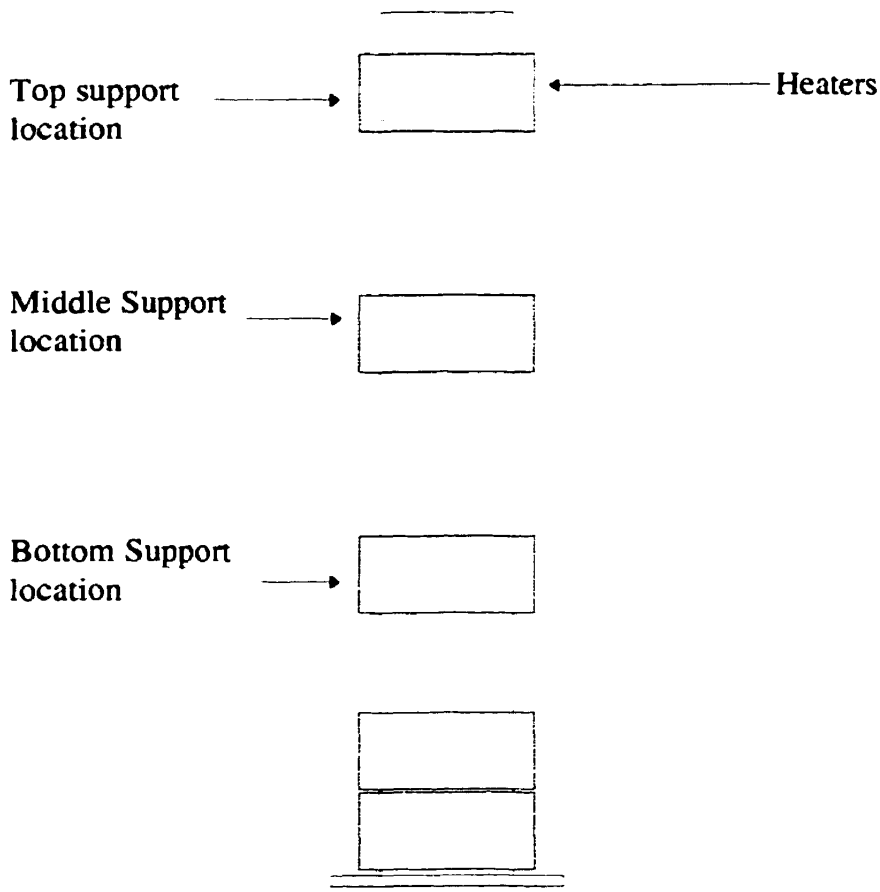

Figure 3.13: MTMDR Heater Locations

Differences Between the RTMDR and MTMDR

Access to the tube and transducers in the RTMDR is limited, since the trough encloses the tube on three sides. The vertical channels in the MTMDR make access to the tube and transducers easier, since there are two open sides. In addition, the channels have holes that allow limited side access.

Sealing the MTMDR for water tests is easier and safer than with the RTMDR. The RTMDR has a front door lid that is clamped shut. Many locations (such as seams in the glass plates of the front door) must be regularly re-sealed. The only sealing location in the MTMDR is where the shell flange meets the finished surface of the baseplate. A groove in the baseplate houses a rubber O-ring that maintains a seal. The flange is held down with eight heavy bolts.

For the RTMDR, the shakers are fastened to a platform on the front door of the rig. The shakers connect to the tube at the top midspan. For the MTMDR, the shakers connect with the collar at the very top of the tube.

Another difference with the MTMDR is that although the same heat exchanger tube was used, space constraints required shortening the overall tube length. The length of each span was therefore shortened. The RTMDR had an overall tube length of 3.74 m. In the MTMDR, each span was 0.915 m long, for an overall tube length of 3.025 m.

The functional advantage of the MTMDR over the RTMDR is the ability to test in water at higher temperatures.

3.2.2 Operation

Based on preliminary RTMDR results analyzed at the time of this testing it was decided that it would be more useful to preload all three supports for MTMDR tests[1]. All three

[1]The RTMDR results suggested that support conditions changed with increasing excitation. The bottom support—centered before the tests and at low excitation levels—became effective as contact occurred at higher levels. This changed the support conditions from two to three spans during testing.

supports were preloaded by adjusting the support platforms so that the tube contacted them with a force of approximately 2 N.

The following steps are similar to those used for the RTMDR (see Subsection 3.1.2). Sensor operation was verified before the shell was placed over the rig and bolted down at the flange. Once the shell was in place shaker rods were connected to the tube collar.

If the test was in water, a nearby water line was inserted into the open top of the shell and the shell filled. If the test was to be in heated water, the heater control unit was turned on, the bottom two heaters were turned on, and the three support heater controls were set to the desired temperature. Once the support location thermocouples registered near the target temperature, the bottom two heaters were turned off.

The heater control system provided accurate water temperatures. Thermocouple measurements indicated that the temperature at any support location never varied by more than 3 °C from the setpoint.

The next step was to turn on the power amplifiers for the shakers and set a power level. Data was recorded on tape for several minutes.

RMS shaker force levels for the MTMDR air and water tests are shown in Tables 3.4 and 3.5.

Table 3.4: MTMDR Air Test Excitation Levels

Test Level	Shaker RMS Force Input Level (N)
1	2.5
2	4.7
3	6.0
4	8.4

Table 3.5: MTMDR Water Test Excitation Levels

Test Level	Shaker RMS Force Input Level (N) at Different Water Temperatures (°C)		
	25	60	90
1	2.2	1.8	1.4
2	3.0	2.9	2.7
3	4.4	4.2	4.3
4	6.3	5.6	5.5

3.3 Data Analysis Method

There were four steps to data analysis, described in Subsections 3.3.1 through 3.3.4.

3.3.1 Analysis Step 1—Calculate Theoretical Vibration Modes

The first step was to calculate vibration frequencies and mode shapes for the test tubes under different support conditions. This did not require test data. The computer program PIPO was used for these calculations (more information on PIPO is given in Section 4.3). Performing these calculations required supplying PIPO with information about tube geometry and support conditions.

3.3.2 Analysis Step 2—Measure Vibration Modes and Damping

The second analysis step was to perform a frequency response analysis of the recorded tube displacement amplitude data. VIVID was the computer program developed to do this analysis (more information on VIVID is given in Section 4.1).

VIVID acquires time-domain midspan vibration amplitude data from the data tape. It then uses the Fast Fourier Transform (FFT) method to calculate the frequency con-

tent of that data. Because of the multi-channel acquisition capability of VIVID, all six midspan displacement signals (two orthogonal directions at each of three midspans for each test) were simultaneously analyzed. The analysis parameters for the tests are given in Table 3.6.

Table 3.6: RTMDR VIVID Parameters

Analysis Parameter (each channel)	RTMDR Tests	MTMDR Tests
Sampling rate	128 Hz	256 Hz
Data window size	2048 points	4096 points
Number of windows	10 or 18	35
Data window	Hanning	Hanning

VIVID acquired 16-second windows (data window size divided by sampling rate) of time-domain data for all midspans and performed the FFT calculations necessary to obtain a frequency response spectrum. This process of capture and analysis was repeated for a number of windows. An average resultant response spectrum was calculated.

The analysis parameters used for the RTMDR tests were based on the maximum available computer memory. Higher sampling rates or larger windows caused program execution errors. No significant aliasing errors were expected, however. According to the results of PIPO[2] the sampling rate of 128 Hz is still greater than twice the frequencies of the first three modes for any support configurations in air or water.

A ten-window average was the largest number possible with the amount of data recorded. The RTMDR tests were the first done and the duration of test data had to be estimated.

Prior to the MTMDR tests, memory was added to the analysis computer. This

[2]See Table 5.1.

allowed the sampling rate and window size parameters for the MTMDR test analyses to be increased. The duration of recorded test data was also increased so that the number of averages could be increased.

The Hanning window mentioned in Table 3.6 is a digital manipulation of the sampled signal in an FFT analysis. The window forces the first and last samples of the time record to zero amplitude. This compensates for an inherent error in the FFT algorithm. The FFT algorithm assumes that the time-domain signal it analyzes is periodic. If the time-domain sample being analyzed does not contain an integral number of cycles, the periodic cycle of the sample will contain discontinuities. These discontinuities cause the energy at specific frequencies to be "spread out" (spectral leakage).

Damping ratios from amplitude frequency response peaks were calculated for every displacement signal spectrum with one or more visually distinguishable peaks. If the program converged on a solution for the damping ratio, the frequency where the peak occurred and the damping ratio were recorded.

3.3.3 Analysis Step 3—Measure Input Energy and Work-Rates at Supports, and Estimate Damping

The third step was to perform work-rate measurements from the recorded tube support forces and motions, and from the shaker input energy. The program developed to do this—WAVI—is described in more detail in Section 4.2 and Appendix C.

WAVI simultaneously acquires four channels of time-domain data (two displacements and two forces). For support work-rates the displacements are of the tube and the forces are those measured in the sensors around the support. For input power to the tube, the displacements and forces are those of the random excitation of the shakers.

All analysis was done from taped data acquired at 8192 Hz (each channel) for a duration of 1 second. Displays of the orbital path of the acquired displacements (part of WAVI's results) indicated that this was a sufficient sample length to characterize the

random motion of the tube in its support. WAVI calculated work-rate (or input power) based on these signals and displayed the results. This 1-second analysis was repeated at least four times for each support or shaker input. The results for each test condition were averaged.

A damping ratio was also calculated from the dissipated shaker input energy using the shaker input power and Equation 2.8.

3.3.4 Analysis Step 4—Calculate Expected Damping Ratios

The final analysis step was to calculate expected damping ratios from the equations of Subsection 2.2.2.

Chapter 4

Analysis Tools

Three computer programs were used to collect and analyze the test data: PIPO, VIVID and WAVI. VIVID and WAVI were specially developed for this study. VIVID acquires the test data, calculates the tube midspan vibration amplitudes, and calculates and plots the corresponding frequency response spectra. It also calculates damping by curve-fitting the spectral peaks. WAVI acquires the test data and calculates the work-rates at the supports and at the excitation shakers. PIPO was used to calculate the natural frequencies and the mode shapes of the multispan tubes. These calculations were compared with the results of VIVID.

4.1 Virtual Instrument for Vibration and Integrated Damping (VIVID)

Measuring the frequency spectra of multispan tube responses is computationally intensive. Analog-to-digital signal conversion and computer programs were used to maximize analysis efficiency.

LabVIEW is a versatile software tool for data acquisition, analysis, and process con-

trol[1]. When this work was initiated, VTU was in the process of implementing LabVIEW in several programs. LabVIEW programs were also developed for this study.

4.1.1 Implementation

The main requirements for data analysis were:

- multiple-channel signal input,
- spectral analysis (e.g., Fast Fourier Transform, or FFT),
- an operational choice to acquire data through analog-to-digital (A/D) conversion from an external source or read a data file of previously acquired and saved results,
- analysis capability to calculate RMS values within variable spectral bandwidths and to perform spectral data curve fits to estimate system parameters like natural frequency and damping ratio, and
- all of the above in an integrated program.

LabVIEW programs are called virtual instruments (VIs) because the user interface on the computer screen resembles an actual instrument with controls and indicators. A VI called as a subroutine from another VI is called a subVI.

Decisions about how the analysis program should be structured resulted in the hierarchy shown in Figure 4.1.

LabVIEW's structure is modular and hierarchical. Repetitive tasks or distinct levels of operation separate easily into subVIs. LabVIEW subVIs connect more visibly than do subroutines in text-based languages, and the hierarchical structure of the entire program is easily seen.

LabVIEW contains a program named SPECTRUM ANALYZER EXAMPLE that meets some of the requirements. SPECTRUM ANALYZER EXAMPLE computes the frequency

[1]See Appendix A.

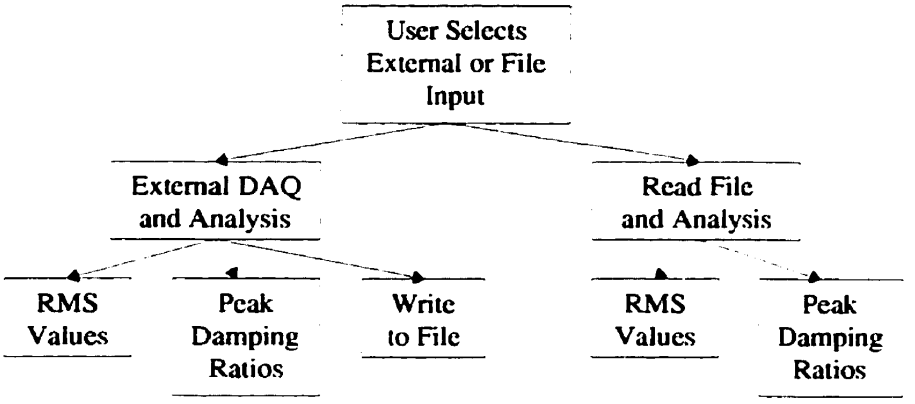

Figure 4.1: Hierarchy of LabVIEW Vibration Analysis Program

spectrum of a single analog signal. It can continuously process signals or capture a single frame of data. It displays each time-domain data window and the calculated frequency spectrum on-screen.

Modifications to SPECTRUM ANALYZER EXAMPLE

Several modifications were made by the author to the SPECTRUM ANALYZER EXAMPLE VI:

1. *Multi-channel capability.* The control for setting the analog input channel on the VI was replaced with a control that accepted a range of channels. SubVIs were already configured to acquire multiple channels.

2. *Write the results to a data file.* A control was added to the VI so that a user may—at any time after acquisition—write a text file to disk that contains acquisition parameters and spectral results. This file can be read by the data file analysis version of the program. It can also be read by any word processor or spreadsheet application.

3. *Read from a data file.* A version of the program to read from a file was created by making a duplicate of the SPECTRUM ANALYZER VI, removing the parts that

acquire signals from the DAQ card and replacing them with subVIs to read text files. The program identifies those lines of the file that are header information and those that are data points.

4. *Calculate RMS values.* Root-mean-square values of a signal within a given frequency bandwidth can be measured by taking the square root of the sum of all the discrete values of the signal power spectrum within that bandwidth. An RMS value within the entire bandwidth is calculated automatically by performing this operation on every point in the spectrum. Cursors on the amplitude spectrum graph allow the user to measure the RMS value for any frequency.

5. *Estimate damping.* VTU uses a FORTRAN code (2PEAK) that uses numerical iteration to solve the damping equation. This method required acquiring data, writing it to a file, and then executing 2PEAK to read the file and output results. The numerical method used (the Marquardt algorithm for least-squares estimation of nonlinear parameters[2]) was translated into equivalent LabVIEW code to be available as a subVI from the main user interface[3].

Results

The modifications listed above resulted in Virtual Instrument for Vibration and Integrated Damping, or VIVID. When used with the base LabVIEW for Windows program and a data acquisition card it accomplishes all the acquisition and analysis requirements. A sample of VIVID output can be seen in Figures 5.1 and 5.2.

[2]See Subsection 2.3.2.
[3]See Section B.2 in Appendix B.

4.2 Work-Rate Analysis Virtual Instrument (WAVI)

A work-rate measurement tool was also required. To do this, a method of measuring work-rates at tube supports and at the point of excitation was developed.

4.2.1 Implementation

A work-rate analysis computer code already existed in VTU as part of a fretting-wear program. That code, named Work-Rate Analysis Program (WRAP), is a LabVIEW VI that measures work-rates from contact between a single heat exchanger tube and its support. The force and displacement transducer assembly used for the fretting-wear rig support is the same as that used in both multispan damping rigs. WRAP was modified by the author to create a multispan work-rate measurement program.

Modifications to WRAP

WRAP was originally developed to run under LabVIEW on a Macintosh computer. The first step was to translate WRAP to a Windows PC platform. LabVIEW VIs are directly portable between the two platforms.

WRAP calculates work-rates for a tube in a support with instrumentation identical to that of the multispan rigs. Little modification was necessary to the calculation portions of the program. There were three main modifications:

1. *Interactive user-defined contact criterion.* When WRAP is used to estimate work-rate, the program applies a contact criterion to the force data. If a force data point falls above a certain user-defined level, contact is considered to have occurred. If the data point falls below that force threshold, it is assumed no contact occurred. This eliminates noise effects in the force signals. This contact criterion is defined as a percentage of the maximum force signal. It is input by the user before the program begins. This requires that the user have an idea of the form of the force

signal before it is acquired. For WAVI, an interactive program step was included to display the entire sampled force signal after acquisition. This allows the user to interactively set a contact criterion level.

2. *VI for shaker work-rates.* Since the rate of energy supplied to the tube by the shakers is measured, a subVI to measure work-rate from the shakers was developed. This subVI is similar in form to the one that calculates work-rates at the supports. Here, however, the work-rate calculated is the power transferred from the shakers to the tube.

3. *Output format.* A different output format was developed for WAVI. Some results were re-ordered and re-labelled from their WRAP format. Other calculation steps—such as the force signal after the contact criterion has been applied, and an X-Y orbital plot of the support or shaker displacement—were included.

Results

These modifications resulted in the Work-rate Analysis Virtual Instrument, or WAVI. When used with the base LabVIEW for Windows program and a data acquisition card it accomplishes all work-rate measurement requirements. A sample of WAVI output can be seen in Figure 5.3.

4.3 Vibration Analysis Code (PIPO)

PIPO is a modification of the original French word for the code, "Pipeau," meaning, roughly, "small pipe". PIPO is a VTU computer code for heat exchanger vibration analysis. It can calculate natural frequencies, mode shapes, and amplitude response levels for flow-excited heat exchanger tubes of any configuration. For this study, PIPO was used to provide analytical values for natural frequencies and mode shapes for each

of the tubes tested. These values were compared with the frequencies measured using VIVID.

Chapter 5

Results and Calculations

The experimental data is presented in this chapter.

In the first section, RTMDR tube frequencies are calculated using PIPO. This section also shows how damping is calculated with VIVID. It also contains measurements of work-rates and damping estimates made from these measurements. Finally, the simplified equations of Subsection 2.2.2 are used to calculate the expected total damping.

The second section contains corresponding results from the MTMDR tests.

5.1 RTMDR

5.1.1 Vibration Analysis using PIPO

RTMDR tests were carried out in air and water at room temperature. Since all, some, or none of the tube supports may be effective[1] in any vibrating condition, there are several possible support configurations. The calculated natural frequency results from PIPO for the first five modes of vibration at different support conditions are shown in Table 5.1. Different support conditions are indicated in this table by a graphic representation of the vertical RTMDR tube and its supports. In each case the tube is shown as effectively

[1]See Figure 2.1 for the definition of an effective support.

supported (⋈ symbol) or unsupported (| symbol) at its top, middle, and bottom support locations.

Table 5.1: Calculated Frequencies (Hz) for the RTMDR—PIPO

Medium	Mode No.	⋈ ⋈ ⋈	⋈ ⋈ |	⋈ | ⋈	| ⋈ ⋈	⋈ | |	| ⋈ |	| | ⋈	| | |
Air	1	29.2	13.2	13.2	6.5	4.7	12.7	9.0	1.1
	2	42.4	36.1	36.1	35.0	15.3	30.9	29.6	6.7
	3	58.2	52.7	52.7	50.4	31.9	42.4	50.3	18.9
	4	112.9	78.8	78.8	61.2	54.5	76.8	69.1	36.9
	5	137.3	125.9	125.9	123.6	83.1	115.9	113.5	61.1
Water	1	22.2	9.6	9.6	5.0	3.6	9.6	6.8	0.8
	2	32.2	23.5	23.5	26.6	11.6	23.5	22.4	5.1
	3	44.2	32.2	32.2	38.3	24.2	32.2	38.2	14.3
	4	85.7	58.3	58.3	46.4	41.3	58.3	52.4	28.0
	5	104.2	88.0	88.0	93.8	63.1	88.0	86.2	46.3

5.1.2 Vibration Modes and Damping Ratios Measured with VIVID

An example of VIVID's output is shown in Figure 5.1. This figure shows the last acquired time-domain data window and the average frequency response spectrum for all windows.

Vibration frequencies and damping ratios were measured with VIVID from these spectra. A sample of the curve fit calculated by VIVID is shown in Figure 5.2. This figure shows a single peak, selected from the spectrum by the user. The calculated spectrum points, a best-fit curve, and the resultant parameters are shown.

Vibration frequency and damping ratios for all RTMDR tests are shown in Table 5.2. These values are the averages of all midspan amplitude spectra with distinguishable peaks (i.e., up to six spectra, two directions at each midspan). Blank entries indicate that VIVID analysis found no distinguishable peaks.

Table 5.2: RTMDR Frequencies and Damping Ratios

Test Medium	Shaker Power Level	Vibration Frequency (Hz)	Damping Ratio (%)
Air	1	11.6	6.7
	2	13.2	2.3
	3	31.0	8.1
	4		
Water	1		
	2	23.9	8.7
	3	24.3	10.2

5.1.3 Midspan Amplitudes for Water Tests Measured with VIVID

Midspan amplitudes were measured for all water tests to calculate energy dissipation due to viscous damping. Those measurements are given in Table 5.3.

Table 5.3: RTMDR Midspan Amplitudes

Shaker Power Level	Top Midspan Amplitude (μm)	Middle Midspan Amplitude (μm)	Bottom Midspan Amplitude (μm)
1	60	38	40
2	287	180	219
3	477	260	345

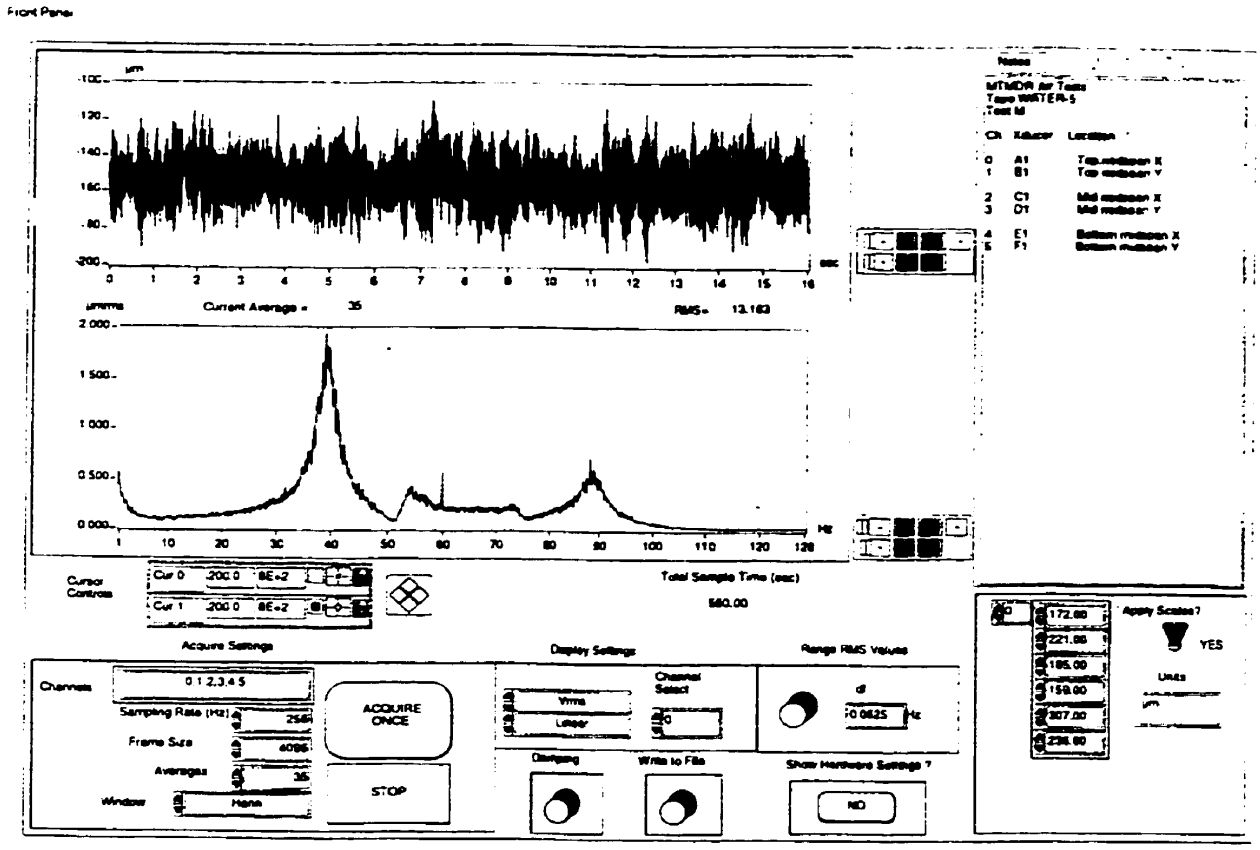

Figure 5.1: Sample VIVID Output—Frequency Response Spectrum

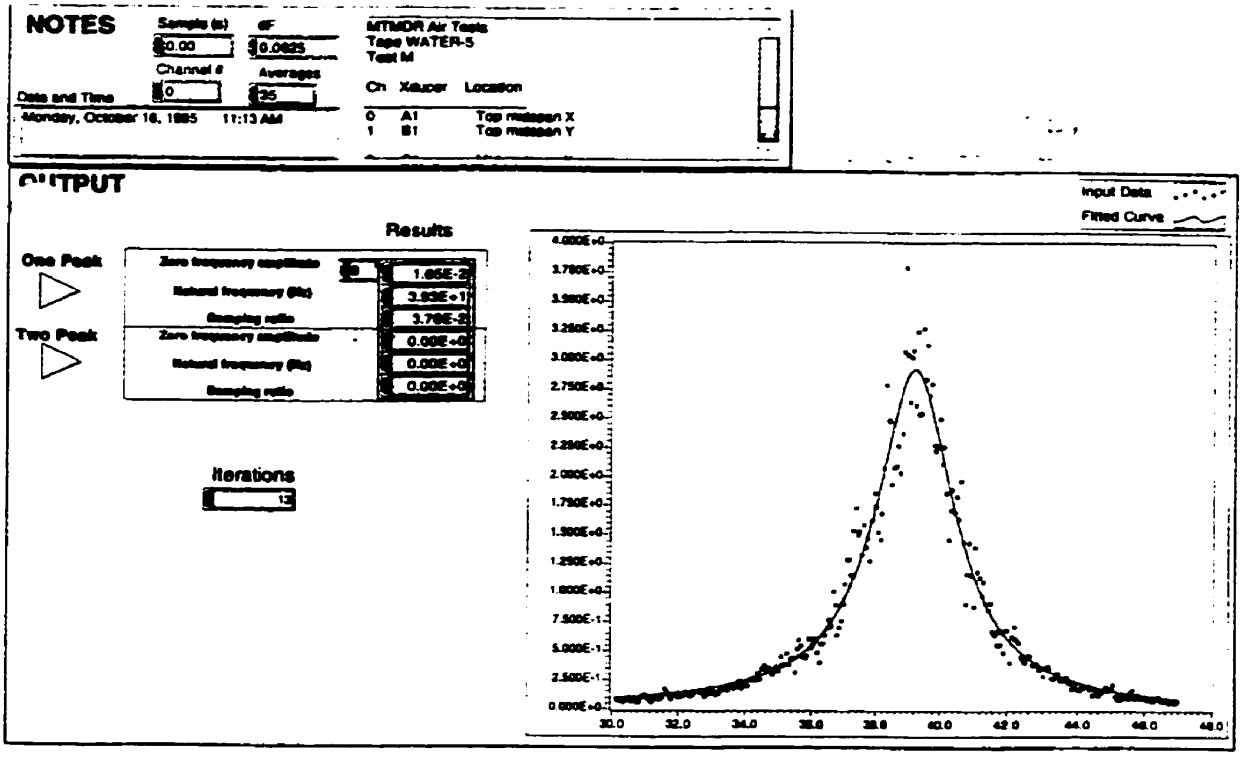

Figure 5.2: Sample VIVID Output—Spectral Peak Curve-Fit

5.1.4 Input Energy and Support Work-Rates Measured with WAVI

Work-rates measured with WAVI for the RTMDR tests are summarized in Tables 5.4 and 5.5. The total support work-rate is the sum of the work-rates measured for all three support locations. Examples of WAVI output with these measurements are shown in Figures 5.3 and 5.4.

Table 5.4: RTMDR Air Test Work-Rate Measurements

Test Level	Total shaker input power (mW)	Total support work-rate (mW)
1	1.0	0.5
2	5.6	3.7
3	12.1	10.1
4	29.2	27.3

Table 5.5: RTMDR Water Test Work-Rate Measurements

Test Level	Total shaker input power (mW)	Total support work-rate (mW)
1	1.9	1.1
2	30.8	16.2
3	107.5	68.7

Work-rate measurements follow expected trends. Increasing the power to the shakers increases work-rate at the shakers. Increasing shaker power also produces greater work-rates at the supports.

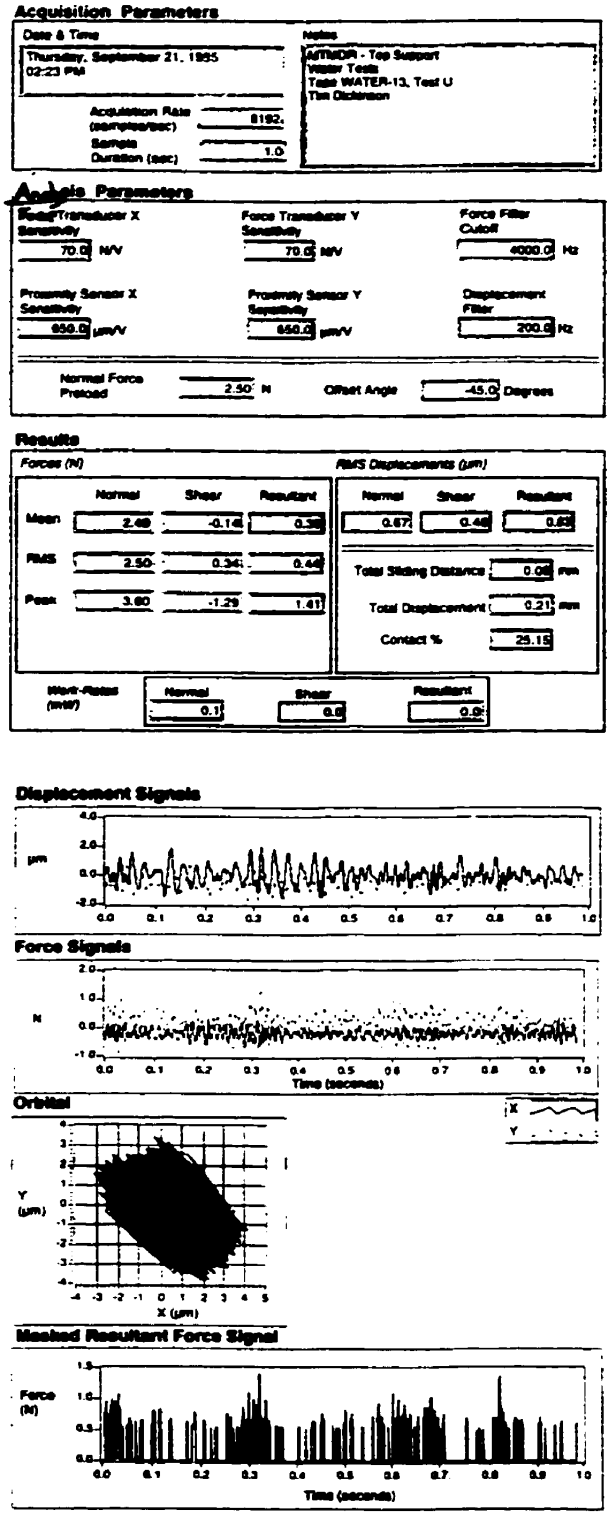

Figure 5.3: Sample WAVI Output—Support Work-Rate

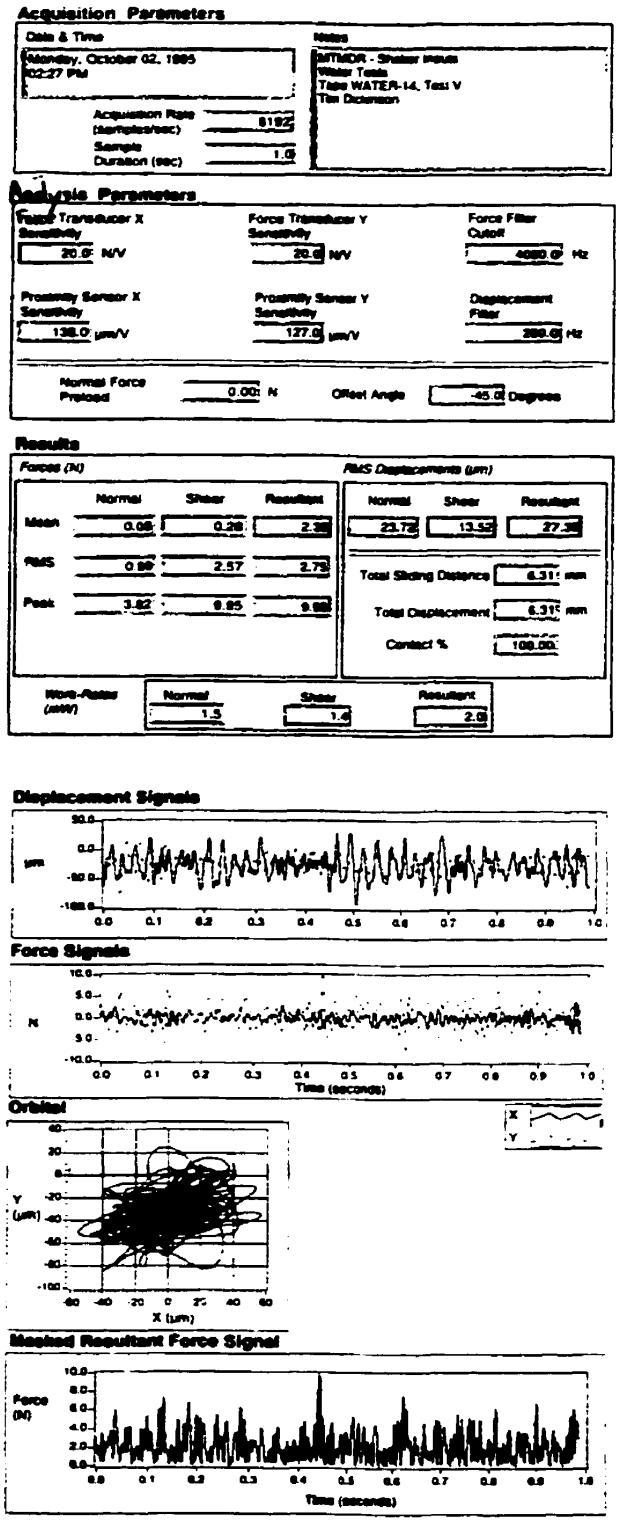

Figure 5.4: Sample WAVI Output—Shaker Input Energy

Damping Ratio Estimates from Input Work-Rates

The effective mass expression

$$\begin{aligned} m &= m_{\text{tube}} + m_{\text{liquid inside tube}} + m_{\text{hydrodynamic}} \\ m &= \rho_{\text{tube}} \frac{\pi}{4} \left({D_o}^2 - {D_i}^2 \right) + \rho_{\text{liquid}} \frac{\pi}{4} {D_i}^2 + c_m \rho_{\text{liquid}} \frac{\pi}{4} {D_o}^2 \end{aligned} \tag{5.1}$$

can be simplified by the small confinement ratio value. The confinement effect c_m is

$$c_m = \frac{1 + \left(\frac{D}{D_e}\right)^2}{1 - \left(\frac{D}{D_e}\right)^2}$$

and since $\frac{D}{D_e}$ is small (the tube is several diameters away from the rig walls) , c_m is approximately 1.0 and the mass Equation 5.1 becomes

$$m = \rho_{tube} \frac{\pi}{4} \left({D_o}^2 - {D_i}^2 \right) + \rho_{liquid} \frac{\pi}{4} \left({D_o}^2 + {D_i}^2 \right)$$

From published water property tables [17] and the tube properties found in Table 3.1 the tube density (ρ_{tube}) is 7944 kg/m^3, the water density is ($\rho_{water@25\,^\circ\text{C}}$) is 997 kg/m^3, the tube outer diameter (D_o) is 15.9 mm, the tube inner diameter (D_i) is 13.7 mm, and the water viscosity (ν) is 0.906 $\times$ 10^{-6} m^2/s, from which the effective mass per unit tube length is

$$m = 0.751 \text{ kg/m}$$

From Equation 2.9, the effective mass of an RTMDR span is then calculated to be:

$$\begin{aligned} m &= \int_0^{1.219} 0.751 \sin^2 \left(\frac{\pi x}{1.219} \right) \mathrm{d}x \\ m &= 0.458 \text{ kg} \end{aligned}$$

In Subsection 2.4.1 it was assumed that the amplitude of vibration is twice the RMS value. As an example calculation, the results from Test Level 1 of the RTMDR water test midspan amplitudes are:

$$\begin{aligned} 60\,\mu\text{m} \times 2 &= 120\,\mu\text{m} \quad \text{at the top midspan} \\ 38\,\mu\text{m} \times 2 &= 76\,\mu\text{m} \quad \text{at the middle midspan} \\ 40\,\mu\text{m} \times 2 &= 80\,\mu\text{m} \quad \text{at the bottom midspan} \end{aligned}$$

The average vibration amplitude is:

$$\frac{120 + 76 + 80}{3} = 92\,\mu\text{m}$$

From Table 5.5 the shaker input power for Test Level 1 in water is 1.9 mW. At a measured frequency of 24 Hz, this corresponds to an energy input of 79.2 μJ/cycle.

From earlier calculations, the effective vibrating tube mass per span is 0.458 kg. Thus, for the three spans, the total effective tube mass is 1.374 kg.

From Equation 2.8, the equivalent viscous damping based on dissipated input energy is:

$$\begin{aligned} \zeta &= \frac{79.2 \times 10^{-6}}{8\pi^3 (1.374) (24)^2 (92 \times 10^{-6})^2} \\ \zeta &= 0.048 = 4.8\% \end{aligned}$$

Similar calculations produce total equivalent viscous damping values for each test case for the RTMDR in air and in water. These results are contained in Table 5.6.

Table 5.6: RTMDR Damping Ratio Estimates from Energy Dissipation

Medium	Test level	Total damping ratio (%)
Air	1	1.0
	2	1.0
	3	1.1
	4	1.5
Water	1	4.8
	2	3.1
	3	4.3

5.1.5 Calculated Expected Damping Ratios

For air tests, the only significant form of multispan damping is friction damping. Recalling Equation 2.1, Pettigrew et al.'s guideline for friction damping in a gas, friction damping for the RTMDR in air is

$$\zeta_{f,air} = 5\left(\frac{N-1}{N}\right)\left(\frac{L}{\ell_m}\right)^{\frac{1}{2}} = 5\left(\frac{3-1}{3}\right)\left(\frac{0.0254}{1.219}\right)^{\frac{1}{2}} \approx 0.5\%$$

This is also the total significant damping for the RTMDR tube in air.

For water tests all three forms of damping are significant: friction, viscous, and squeeze-film.

To apply the design recommendations of Subsection 2.2.2, the Stokes number must be greater than 3300 and the confinement ratio must be much less than 0.5. The limiting case for the Stokes Number is the lowest measured frequency of 12 Hz[2]. From Equation 2.4 the Stokes Number is

$$S = \frac{\pi(12)\left(15.9\times10^{-3}\right)^2}{2\left(0.9\times10^{-6}\right)} \approx 5295$$

which satisfies the requirement that S is greater than 3300.

A single tube is being tested and the walls of the rig are several diameters away from the tube. The confinement ratio requirement, $\frac{D}{D_e} \ll 0.5$, is therefore satisfied.

The low confinement ratio can be used to simplify Rogers' formula for viscous damping (Equation 2.3). It becomes:

$$\zeta_\nu = \frac{100\pi}{\sqrt{8}}\left(\frac{\rho_{liquid}{D_o}^2}{m}\right)\left(\frac{2\nu}{\pi f {D_o}^2}\right)^{\frac{1}{2}} \tag{5.2}$$

Substituting the aforementioned water and tube property values into Rogers' simplified equation (Equation 5.2) results in a viscous damping ratio expression (in percent) of:

$$\zeta_\nu = 1.784\left(\frac{1}{\sqrt{f}}\right)$$

[2]See the VIVID analysis for the RTMDR in air in Subsection 5.1.2.

for the RTMDR tube in liquid.

Using this expression for the viscous damping ratio of a tube in a fluid and using the dominant observed frequency of 24 Hz, the RTMDR viscous damping ratio is $\zeta_v = 0.36\%$. Recalling Equation 2.2, Pettigrew et al.'s guideline for friction damping in a liquid, friction damping for the RTMDR in water is

$$\zeta_{f,liquid} = 0.5\left(\frac{N-1}{N}\right)\left(\frac{L}{\ell_m}\right)^{\frac{1}{2}} = 0.5\left(\frac{3-1}{3}\right)\left(\frac{0.0254}{1.219}\right)^{\frac{1}{2}} \approx 0.05\%$$

Recalling Equation 2.5, Pettigrew et al.'s guideline for squeeze-film damping in a liquid, RTMDR squeeze-film damping in water is

$$\begin{aligned}\zeta_{sf} &= \left(\frac{N-1}{N}\right)\left(\frac{1460}{f}\right)\left(\frac{\rho D^2}{m}\right)\left(\frac{L}{\ell_m}\right)^{\frac{1}{2}} \\ \zeta_{sf} &= \left(\frac{3-1}{3}\right)\left(\frac{1460}{24}\right)\left(\frac{997(0.0159)^2}{0.751}\right)\left(\frac{0.0254}{1.219}\right)^{\frac{1}{2}} \approx 2.0\%\end{aligned}$$

These three forms of damping—viscous, friction, and squeeze-film—add for a total damping of 2.4% for the RTMDR tube in water.

5.2 MTMDR

5.2.1 Vibration Analysis using PIPO

The results of PIPO calculations for the MTMDR tube are shown in Table 5.7.

5.2.2 Vibration Modes and Damping Ratios Measured with VIVID

As with RTMDR data, every amplitude spectrum that had one or more distinct peaks was analyzed with the peak-fitting subprogram (see Section 4.1), and natural frequency and damping ratio values were measured. The results are given in Table 5.8. Again, blank entries indicate that the resultant spectra contained no peaks that could be curve-fitted with VIVID.

Table 5.7: Calculated Frequencies (Hz) for the MTMDR—PIPO

Medium	Mode No.	⋈ ⋈ ⋈	⋈ ⋈ |	⋈ | ⋈	| ⋈ ⋈	⋈ | |	| | ⋈
Air	1	48.0	22.5	15.7	7.3	12.1	2.7
	2	70.9	50.5	49.7	48.1	33.5	17.6
	3	100.5	71.3	84.9	71.4	65.6	49.8
	4	126.1	119.0	103.8	101.7	108.4	86.2
	5	217.5	142.3	146.8	158.1	162.0	110.5
Water	1	36.4	17.1	11.9	5.5	9.2	2.0
	2	53.8	38.3	37.7	36.5	25.4	13.4
	3	76.3	54.1	64.4	54.2	49.8	37.8
	4	95.7	90.3	78.8	77.2	82.3	65.5
	5	165.1	108.0	111.4	120.0	122.9	83.9

Table 5.8: Measured MTMDR Vibration Frequencies and Damping Ratios

Test Medium	Shaker Test Level	Vibration Frequency (Hz)	Damping Ratio (%)
Air	1	42.7	9.0
	2	43.6	8.5
	3	44.2	9.7
	4	45.1	8.2
Water at 25°	1	39.1	4.0
	2		
	3		
	4		
Water at 60°	1	38.1	5.0
	2	38.0	5.1
	3	38.3	5.3
	4	37.6	6.0
Water at 90°	1	38.2	5.7
	2	37.4	6.0
	3	37.2	5.8
	4	37.0	6.4

5.2.3 Midspan Amplitudes for Water Tests Measured with VIVID

Midspan amplitudes were measured for all water tests to calculate energy dissipation due to viscous damping. Those measurements are given in Table 5.9.

Table 5.9: MTMDR Midspan Amplitudes

Medium	Shaker Power Level	Top Midspan Amplitude (μm)	Middle Midspan Amplitude (μm)	Bottom Midspan Amplitude (μm)
Water at 25°C	1	21	15	10
	2	38	28	18
	3	60	42	26
	4	78	54	34
Water at 60°C	1	18	13	8
	2	39	27	16
	3	60	40	23
	4	83	52	29
Water at 90°C	1	16	11	7
	2	34	22	12
	3	56	33	18
	4	77	43	24

5.2.4 Input Energy and Support Work-Rates Measured with WAVI

Work-rates measured with WAVI are shown in Table 5.10 (air tests) and 5.11 (water tests).

These measurements follow expected patterns. Increasing shaker power produces increasing work-rates measured at the shakers and at the supports. As with the RTMDR,

Table 5.10: MTMDR Air Test Work-Rate Measurements

Test Level	Total shaker power (mW)	Total support work-rate (mW)
1	0.8	0.4
2	2.1	1.3
3	4.7	3.6
4	8.0	6.2

Table 5.11: MTMDR Water Test Work-Rate Measurements

Water Temperature (°C)	Test Level	Total shaker power (mW)	Total support work-rate (mW)
25	1	0.3	0.0
	2	2.2	0.4
	3	3.9	1.1
	4	6.1	2.2
60	1	0.2	0.0
	2	1.5	0.4
	3	2.4	0.8
	4	5.5	1.7
90	1	0.2	0.0
	2	1.8	0.4
	3	3.2	0.9
	4	4.5	1.7

the sum of the support work-rates in air is slightly less than the shaker work-rates.

Damping Ratio Estimates From Input Work-Rates

Damping ratios from input power dissipation are shown in Tables 5.12 and 5.13. Calculations are the same as those done in Subsection 5.1.4.

Table 5.12: Damping Ratio Estimates from Shaker Work-Rates for the MTMDR in Air

Test level	Total damping ratio (%)
1	2.5
2	2.1
3	2.4
4	2.6

5.2.5 Calculated Expected Damping Ratios

Using Equation 2.1—Pettigrew et al.'s guideline for friction damping in a gas—friction damping for the MTMDR in air is $\zeta_{f,air} = 0.6\%$.

From Equation 2.4), the limiting case Stokes number (i.e., lowest frequency and highest viscosity) is

$$S = \frac{\pi(37.4)\left(15.9 \times 10^{-3}\right)^2}{2\left(0.9 \times 10^{-6}\right)} \approx 16502$$

which is greater than 3300.

Here as well, the confinement ratio $\frac{D}{D_c} \ll 0.5$, since only a single tube is being tested and the walls of the rig are several diameters away from the tube.

Water density, viscosity, and tube effective mass per unit length are shown in Table 5.14. Since the water parameters are temperature-dependent, the effective mass is slightly different for each testing temperature.

Table 5.13: Damping Ratio Estimates from Shaker Power for the MTMDR in Water

Water temperature (°C)	Test level	Total damping ratio (%)
25	1	2.1
	2	4.6
	3	3.6
	4	3.3
60	1	2.1
	2	3.6
	3	2.5
	4	3.3
90	1	2.9
	2	6.3
	3	4.5
	4	3.5

Table 5.14: MTMDR Water Parameters as a Function of Temperature

Water Temperature (°C)	$\rho_{water}\left(\mathrm{kg/m^3}\right)$	$\nu\,(\mathrm{m^2/s})$	$m\,(\mathrm{kg/m})$
25	997.0	0.906×10^{-6}	0.751
60	983.2	0.477×10^{-6}	0.746
90	965.3	0.328×10^{-6}	0.740

Substituting these values into Equation 5.2 results in an expression for MTMDR viscous damping ratio for each test temperature. These expressions are shown in Table 5.15.

Table 5.15: Viscous Damping Ratio Expressions for the MTMDR Tube in Water

Water Temperature (°C)	Viscous Damping Ratio Equation (%)
25	$\zeta_\nu = \frac{1.784}{\sqrt{f}}$
60	$\zeta_\nu = \frac{1.283}{\sqrt{f}}$
90	$\zeta_\nu = \frac{1.052}{\sqrt{f}}$

For the dominant observed frequency of 45 Hz, the MTMDR viscous damping ratios are:

$$\zeta_v \quad \text{at } 25^\circ\text{C} \;=\; 0.3\%$$

$$\zeta_v \quad \text{at } 60^\circ\text{C} \;=\; 0.2\%$$

$$\zeta_v \quad \text{at } 90^\circ\text{C} \;=\; 0.2\%$$

Recalling Equation 2.2, friction damping for the MTMDR in water is $\zeta_{f,liq} = 0.1\%$, and for Equation 2.5, values for MTMDR squeeze-film damping in water are

$$\zeta_{sf} \quad \text{at } 25^\circ\text{C} \;=\; 1.2\%$$

$$\zeta_{sf} \quad \text{at } 60^\circ\text{C} \;=\; 1.2\%$$

$$\zeta_{sf} \quad \text{at } 90^\circ\text{C} \;=\; 1.2\%$$

Total damping ratios for the water tests are 1.6% for tests at 25° C, and 1.5% for tests at 60° C and 90° C.

Chapter 6

Discussion

The results reported previously are discussed in this chapter in light of the objectives of this work.

Output from VIVID and WAVI are sometimes shown in figures in this section for illustration. Examples are not given for every case, since the quantity of results from VIVID and WAVI is too large for complete inclusion in this document.

6.1 Comparing Vibration Frequencies Measured with VIVID and PIPO Results

PIPO is a validated code. Modes calculated with PIPO represent vibrating tubes with clamped and pinned boundary conditions. Although RTMDR and MTMDR tube support conditions are not perfectly clamped and pinned, agreement between frequencies calculated with PIPO and measured with VIVID are evidence that the correct vibration modes are identified.

6.1.1 RTMDR Air Tests

VIVID results show that the top midspan displacement amplitude spectrum is very broad for all frequencies up to about 30 Hz. Above that it drops significantly (see Figure 6.1). This behaviour occurs for all four input power levels. A broad response at the top midspan is due to its proximity to the shaker connection location.

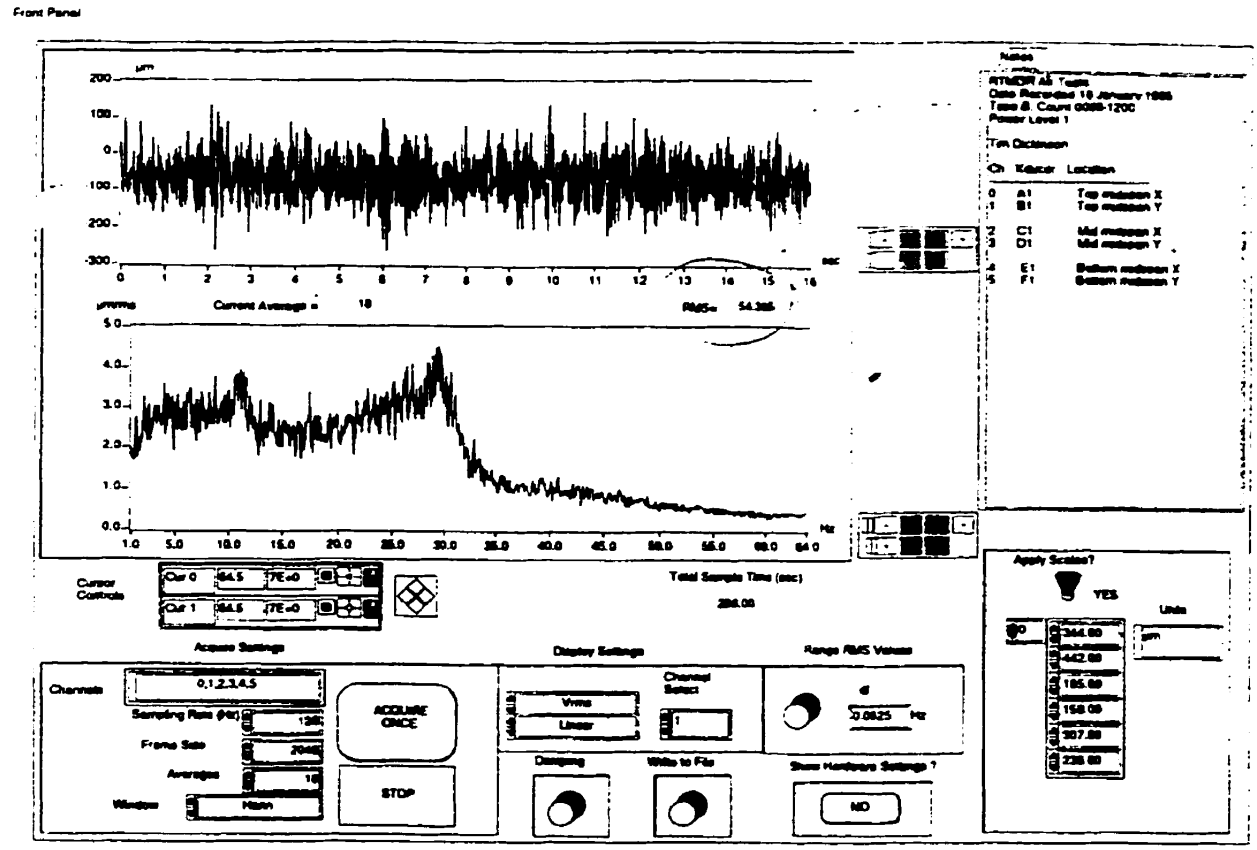

Figure 6.1: RTMDR Air Test Indicating Broad Frequency Response at Top Midspan—VIVID Result

The other midspans show significant response peaks at about 12 Hz, as shown in Table 5.2. An example is shown in Figure 6.2. There are smaller peaks at 30 Hz that increase to surpass the 12 Hz peaks at higher excitation levels (see Figure 6.3—this change is also indicated in Table 5.2). This 30 Hz peak increase occurs at the bottom midspan at

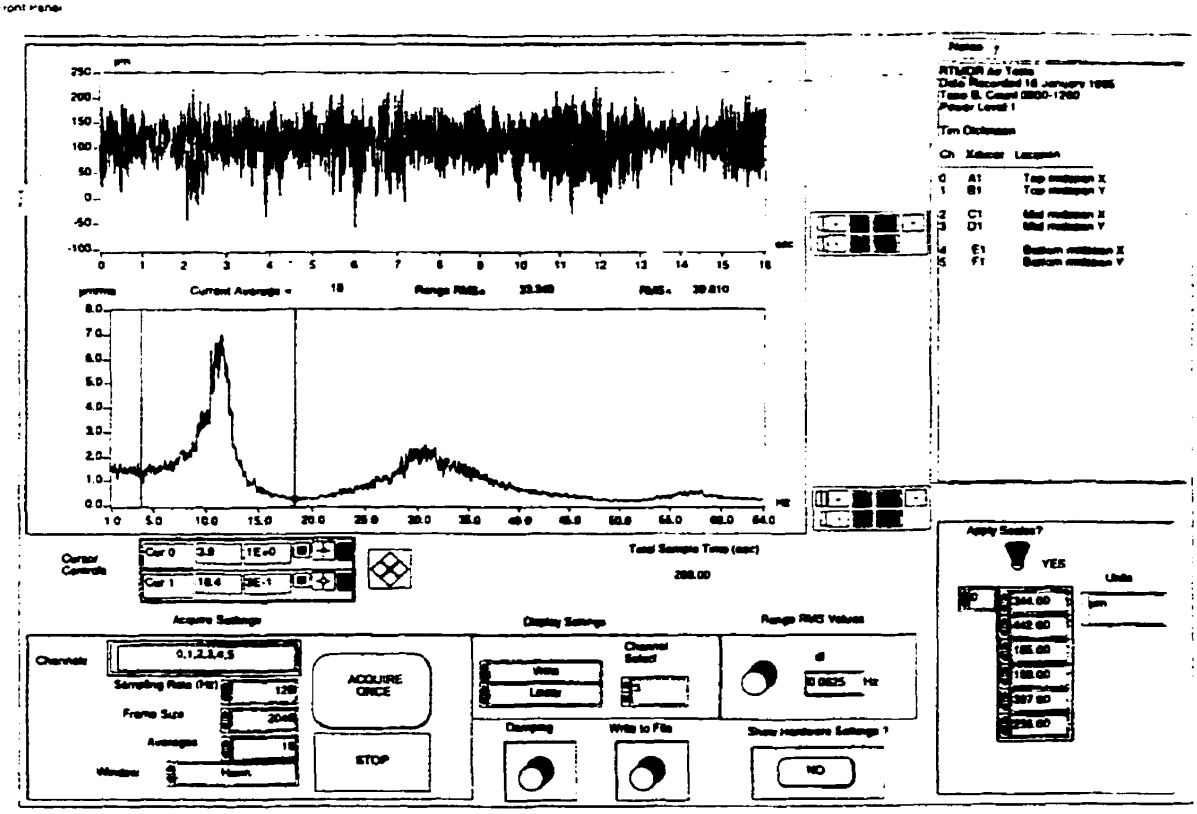

Figure 6.2: RTMDR Air Test 12 Hz Peak at Middle Midspan—VIVID Result

low excitation levels and occurs at the middle and upper midspans at higher excitation levels.

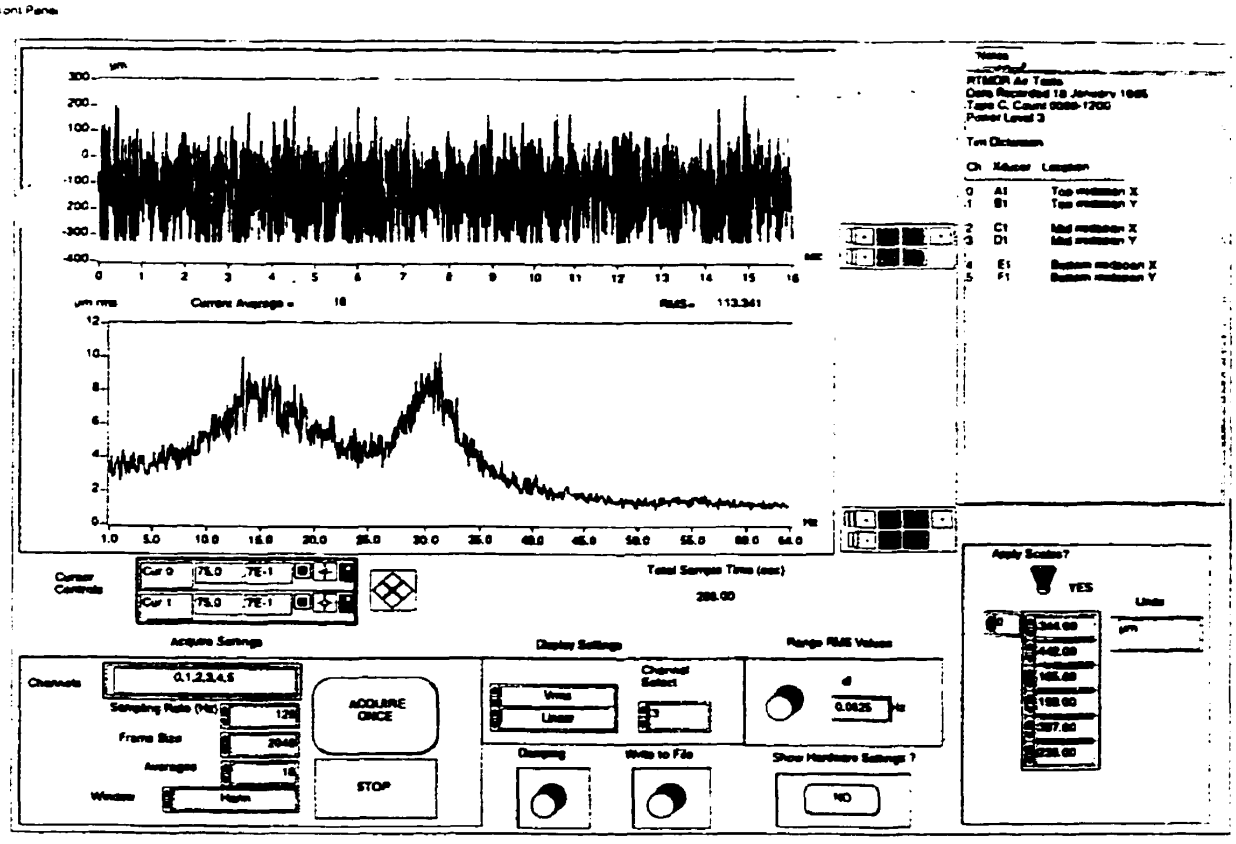

Figure 6.3: RTMDR Air Test 30 Hz Peak Growing with Increased Excitation at Middle Midspan—VIVID Result

PIPO predicts a fundamental natural frequency of 13.2 Hz (Table 5.1) for the case where only the top and middle supports are effective. These values correspond with the 12 Hz response peak seen at low power levels (the bottom support was the only one where the tube was properly centered). At low input forces the tube did not contact the bottom support. The support was ineffective.

At higher excitation levels, as indicated above, the dominant amplitude spectrum peak changed to 30 Hz. The PIPO results of Table 5.1 indicate that the fundamental mode of the all-supports-effective case is very close to this (29.2 Hz). At these levels the

tube is contacting the bottom support more often and all supports are effective.

6.1.2 RTMDR Water Tests

As found in the air tests, the top midspan displacement amplitude spectrum is very broad up to about 25 Hz for all levels (see Figure 6.4).

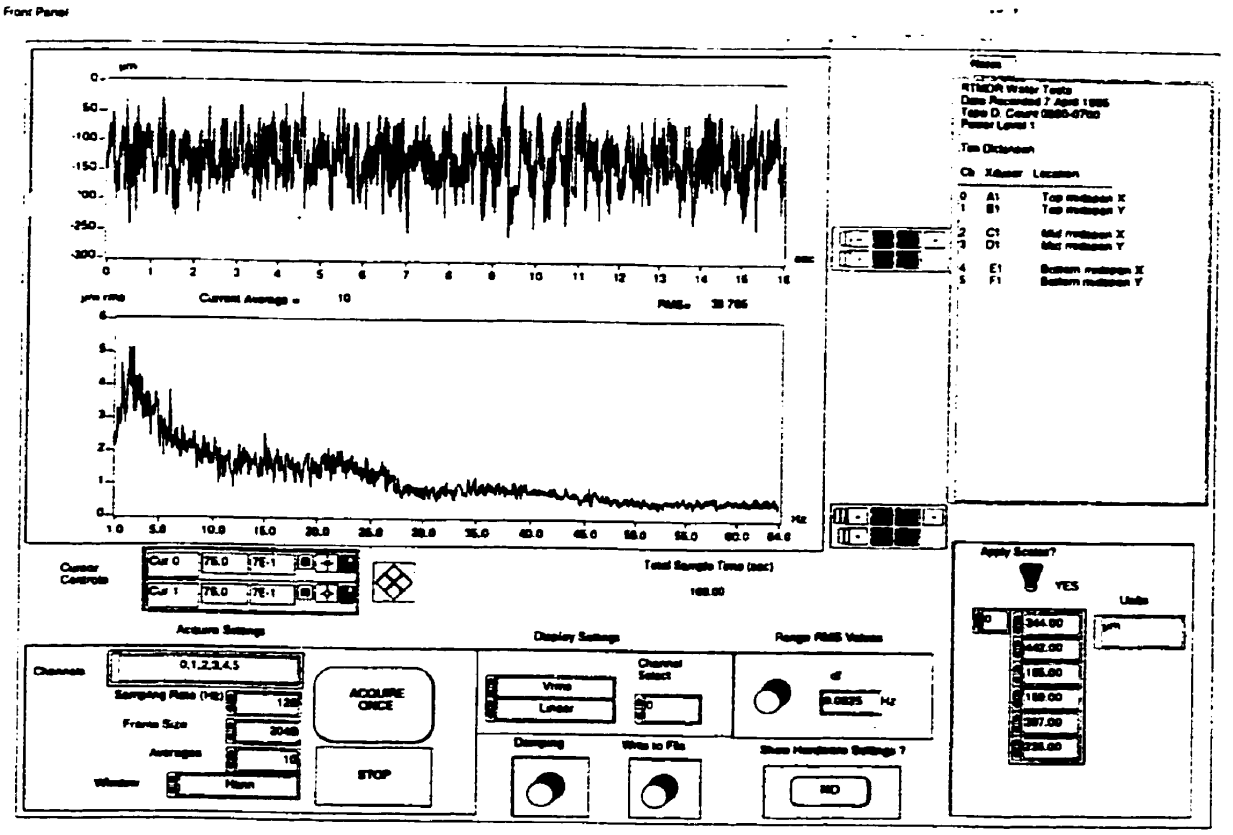

Figure 6.4: RTMDR Water Test with Broad Frequency Response at Top Midspan—VIVID Result

The middle and bottom midspan displacement frequency spectra each show a peak at approximately 24 Hz for all power levels (see Figure 6.5 and Table 5.2).

Table 5.1 indicates that PIPO predicts a fundamental frequency of 22.2 Hz for the all-supports-effective case of the RTMDR in water. This is a reasonable match with the measured frequency since all supports were preloaded.

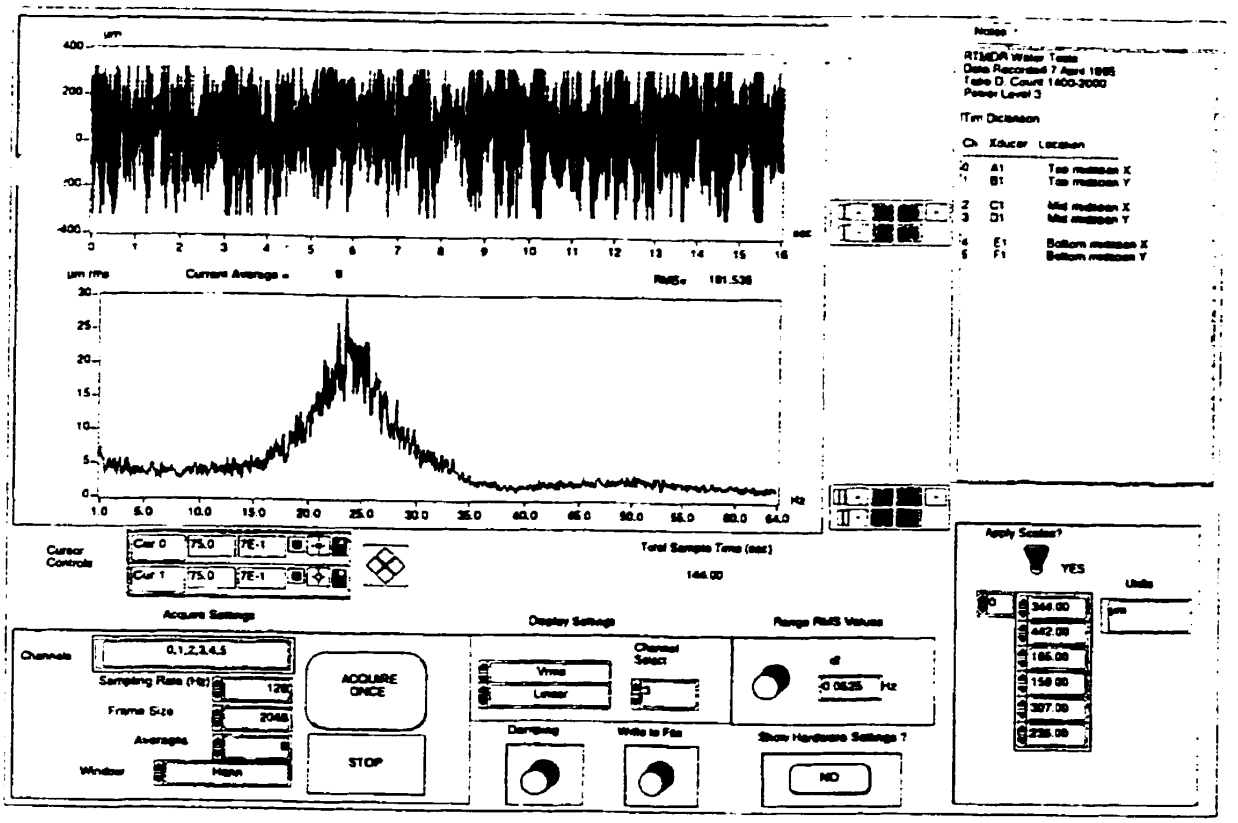

Figure 6.5: RTMDR Water Test 24 Hz Peak at Middle Midspan—VIVID Result

6.1.3 MTMDR Air Tests

Top and middle midspan measurements produced the most distinct vibration peaks. The largest occurs at approximately 43 to 45 Hz. The averages are reported in Table 5.8, and an example is shown in Figure 6.6.

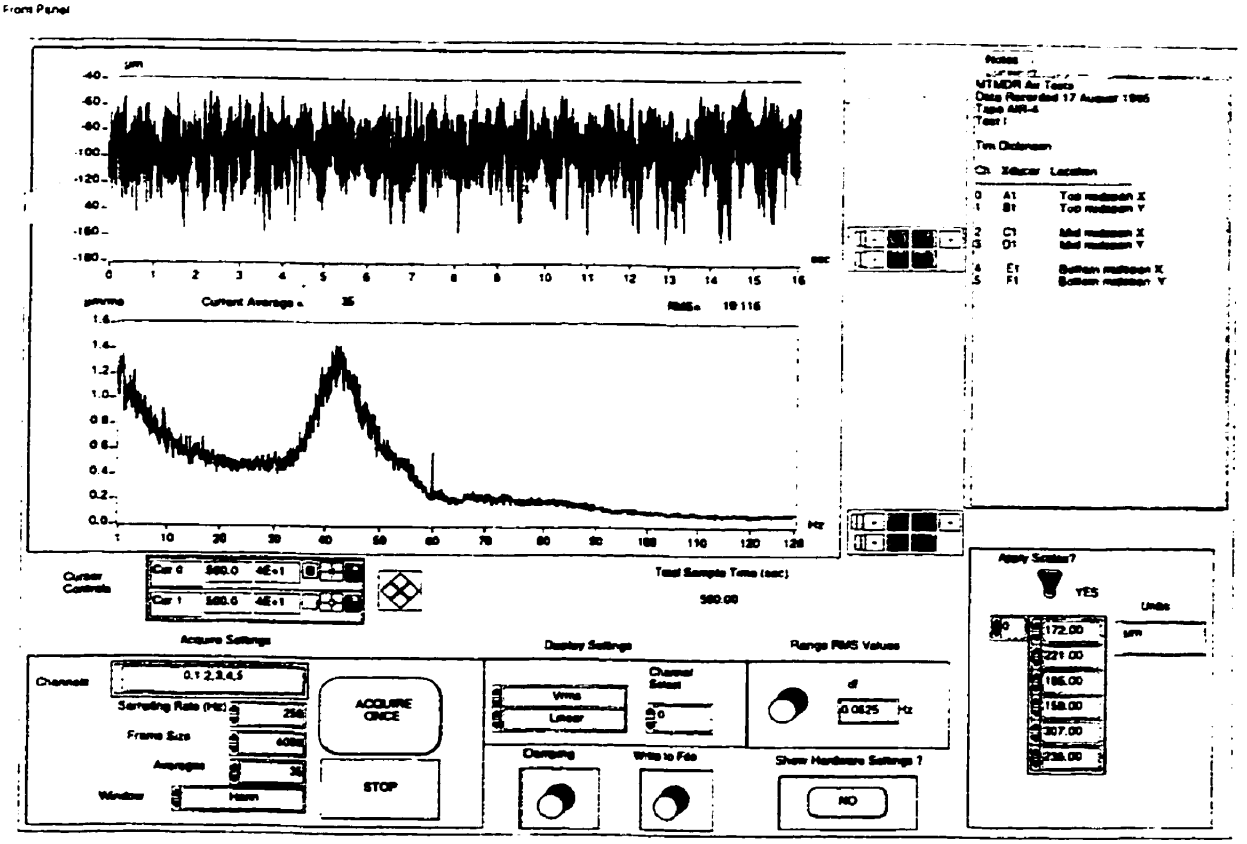

Figure 6.6: MTMDR Air Test 44 Hz Peak—VIVID Result

From Table 5.7, PIPO predicts a fundamental natural frequency of 48 Hz for three effective supports. This is close to the measured value.

6.1.4 MTMDR water tests

The natural frequencies measured in MTMDR water tests using VIVID are shown in Table 5.8. They are all approximately 38 Hz. PIPO predicts a natural frequency of

36.4 Hz for an MTMDR tube in water with all supports effective.

6.2 Damping Ratios Measured with VIVID from Frequency Responses

6.2.1 RTMDR Air Tests

Damping ratios measured with VIVID varied significantly, from 2% to 8%. Averages, again, are in Table 5.2. An example is shown in Figure 6.7.

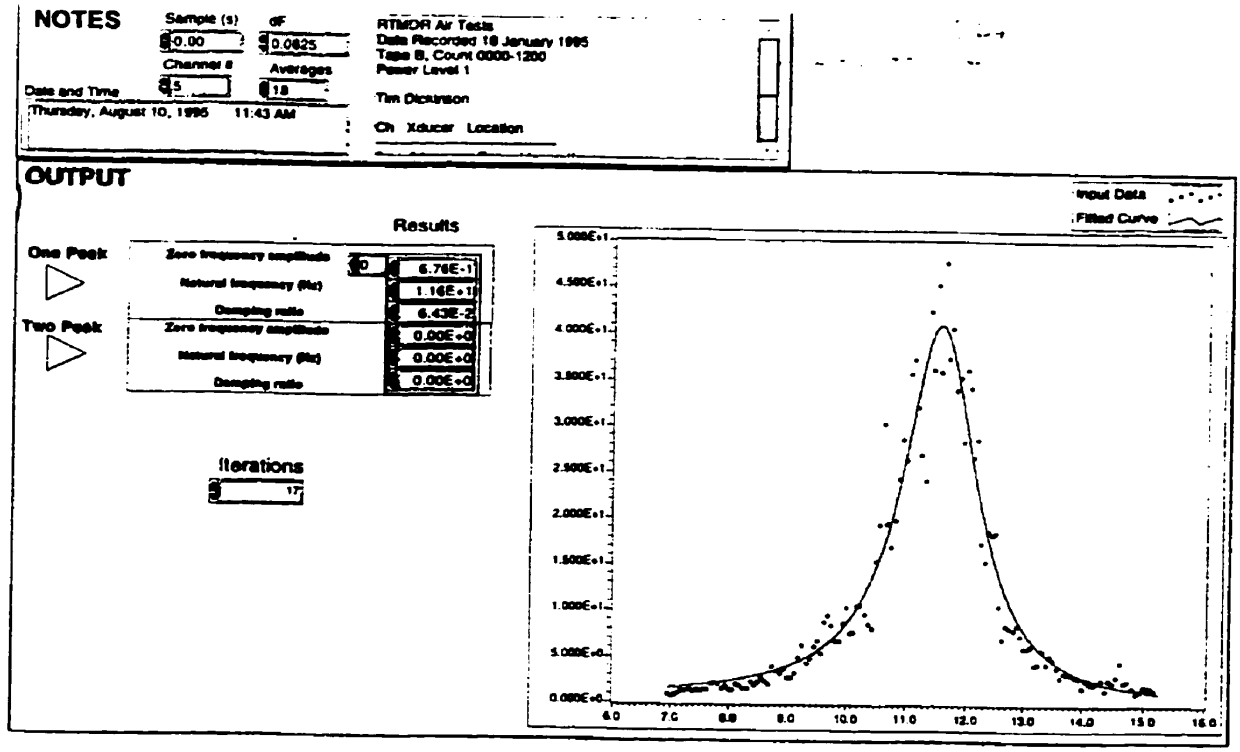

Figure 6.7: Sample RTMDR Air Damping Ratio—VIVID Result

Previous experimentation by Pettigrew et al. [5] indicates that heat exchanger tube damping ratios in air are typically near 1%. One possible reason for the large damping ratios measured by VIVID in these tests is that even the two-peak analysis is a sim-

plification of the non-linear tube dynamics. The non-linearities of a tube contacting its supports at different points, or of different tube material properties, may not be so discrete. A close "cluster" of spectral peaks could emerge that may show up as one or more broadened peaks. Such peaks may still center on the correct frequency. The peak broadness implies an exaggerated damping ratio in the same way that fitting two peaks with a single curve would.

6.2.2 RTMDR Water Tests

As in air tests, damping ratios measured with VIVID in water tests were large—between 8% and 10% as power levels increased (see Figure 6.8 and Table 5.2).

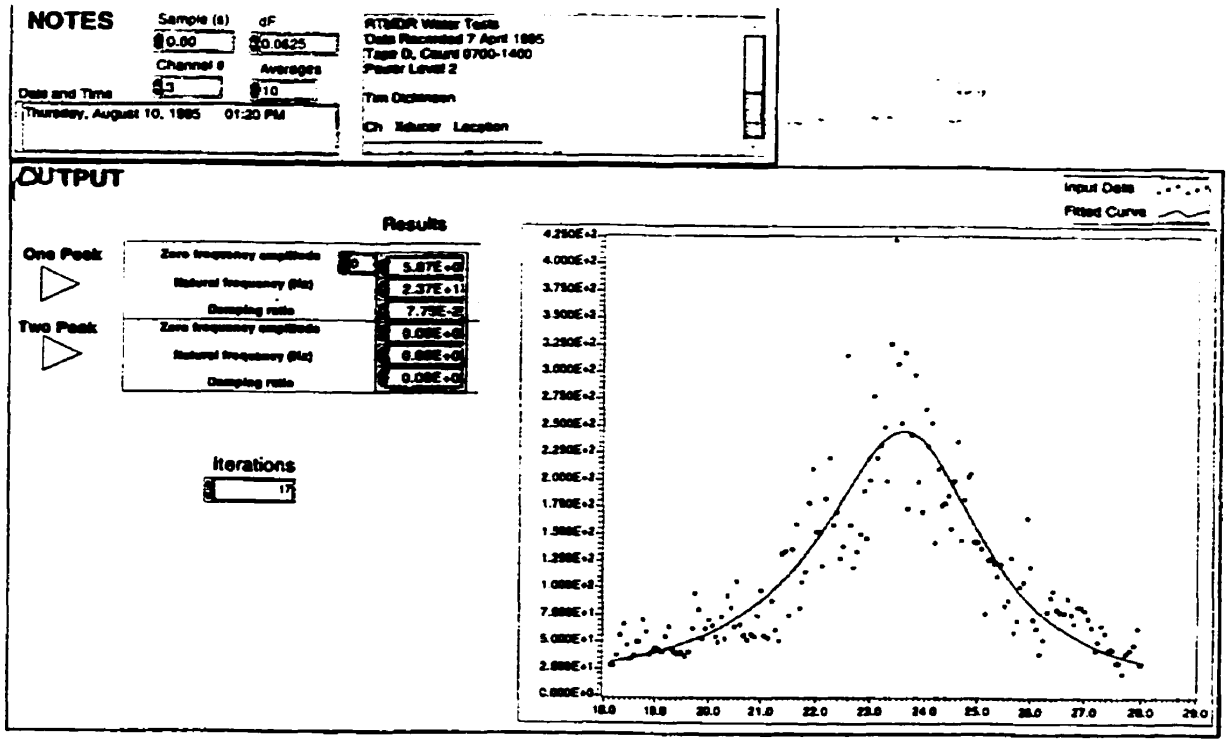

Figure 6.8: Sample RTMDR Water Damping Ratio—VIVID Result

6.2.3 MTMDR Air Tests

Damping ratios measured with VIVID from the top and middle midspan responses varied between 8% and 11%, with averages shown in Table 5.8. These are also larger than the 1% range predicted by Pettigrew et al. The reasons are the same—probably non-linearities of the tube/support interaction.

6.2.4 MTMDR Water Tests

Damping ratios for MTMDR water tests are also given in Table 5.8. Averages range from 4% to more than 6%.

These results are unusual. Damping ratios measured increased slightly with temperature. It was expected that damping would decrease with increased water temperature as water viscosity decreases.

6.3 Damping Ratio Comparisons

Figures 6.9 to 6.14 contain graphs comparing damping ratios calculated or estimated from each of three methods: Pettigrew et al.'s equations, curve-fitting frequency response peaks with VIVID, and the dissipation rate of the input energies measured by WAVI.

In all cases, the graphs indicate that the damping values measured with the two test methods are always greater than Pettigrew et al.'s guidelines. This is expected, since the guidelines are a lower bound of many experimental data and meant to make a conservative (i.e., worst-case) estimate of damping.

At almost every data point, damping measured by spectral peak curve-fits is greater than that estimated from input energy. This is probably due to the aforementioned difficulty in estimating damping from spectral curve-fits: non-linearities contribute to peak broadening resulting in incorrectly large damping estimates. Estimating damping from the dissipated input energy avoids this difficulty, and produces lower damping estimates

that are closer to the guideline values.

There does not appear to be any significant effect of excitation level on damping in any of the graphs (Figures 6.10, 6.12, 6.13, and 6.14). This agrees with the previous experimental data bounded by Pettigrew et al.'s guidelines.

There does not appear to be any significant effect of temperature on damping in the water test results. While this agrees with Pettigrew et al.'s guidelines, it is not immediately clear why there should be no temperature effect. The viscosity of water decreases by a factor of nearly three between 25° C and 90° C. It might be expected that this changing viscosity would have a significant impact on viscous and squeeze-film damping. One possible explanation for the lack of temperature effect is that at higher temperatures the fluid viscosity will be lower, but the fluid film between the tube and support may be thinner. The decrease in damping due to the lower viscosity of the squeezed fluid may be offset by an increase in damping due to the greater constriction of the tube/support gap allowing displacement of the squeezed fluid. The absence of temperature effect is still under investigation, however.

It is important to note that the data reported in the graphs is highly statistical in nature. That is, there are a number of factors (e.g., tube/support preloading or clearances, bent tubes) that can change with every test. These factors can explain the small variations in damping seen between different tests. These factors also imply that these tests form one or two statistical "points" in the group of test data from which Pettigrew et al.'s guidelines were made. The real significance of this work is that these data points were made with a new and improved damping measurement method: the work-rate method.

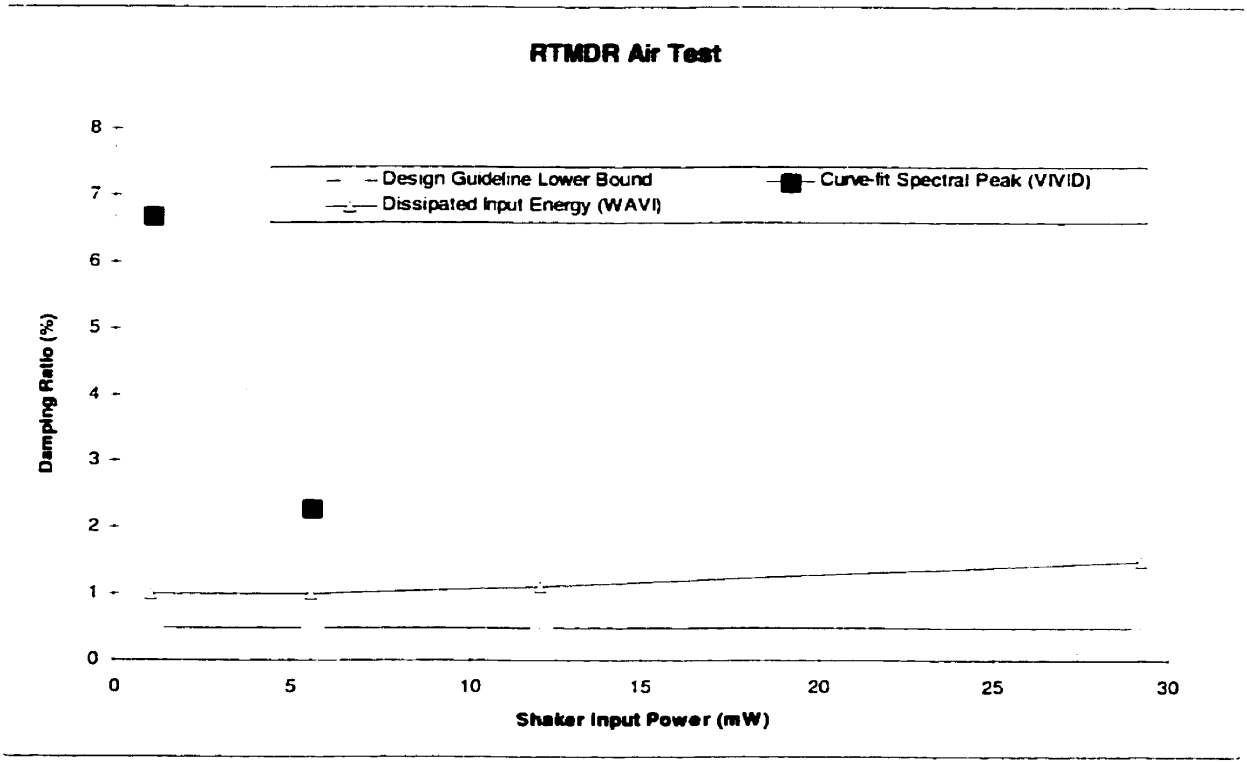

Figure 6.9: RTMDR Air Test Damping Ratios

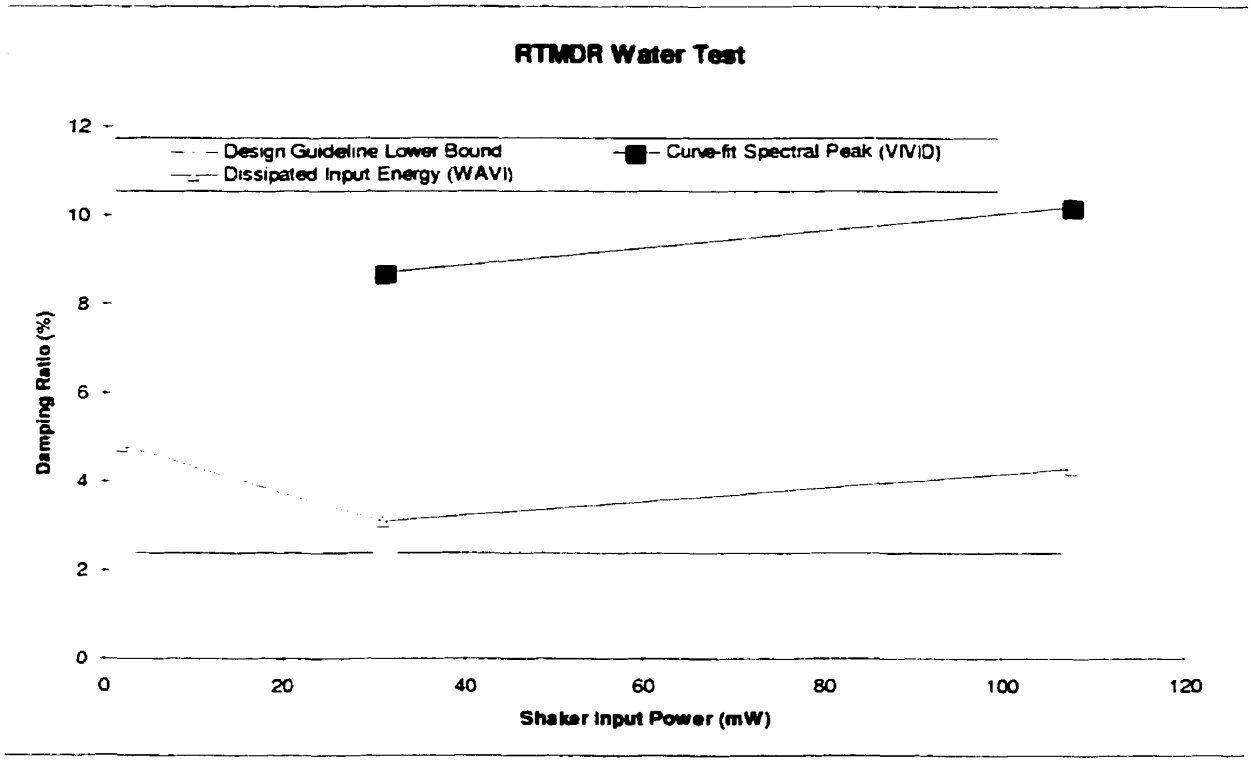

Figure 6.10: RTMDR Water Test Damping Ratios

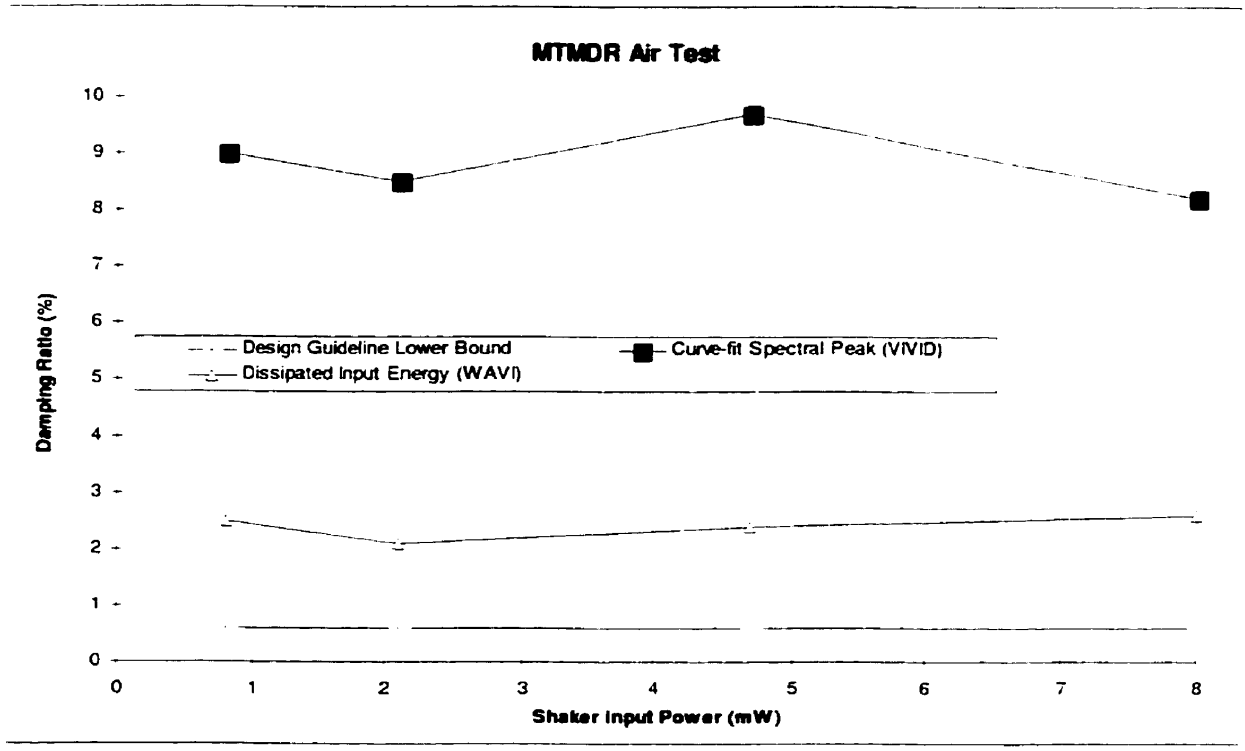

Figure 6.11: MTMDR Air Test Damping Ratios

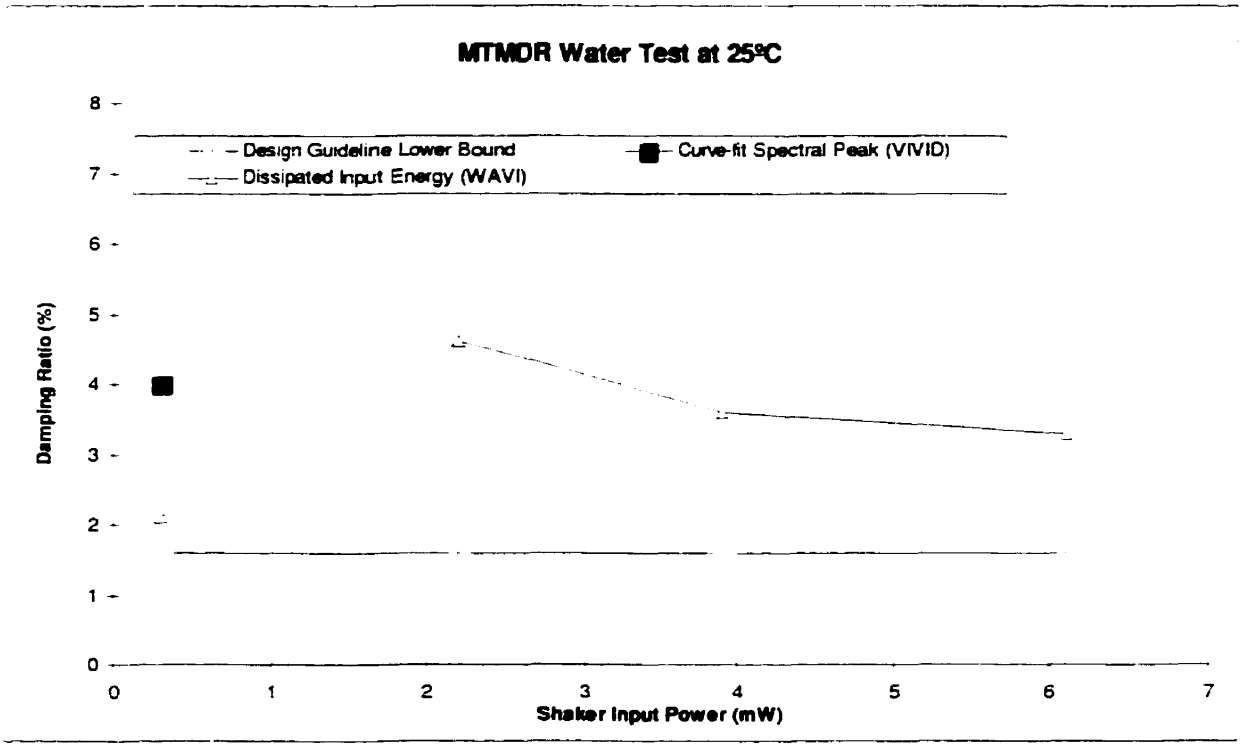

Figure 6.12: MTMDR Water at 25° Test Damping Ratios

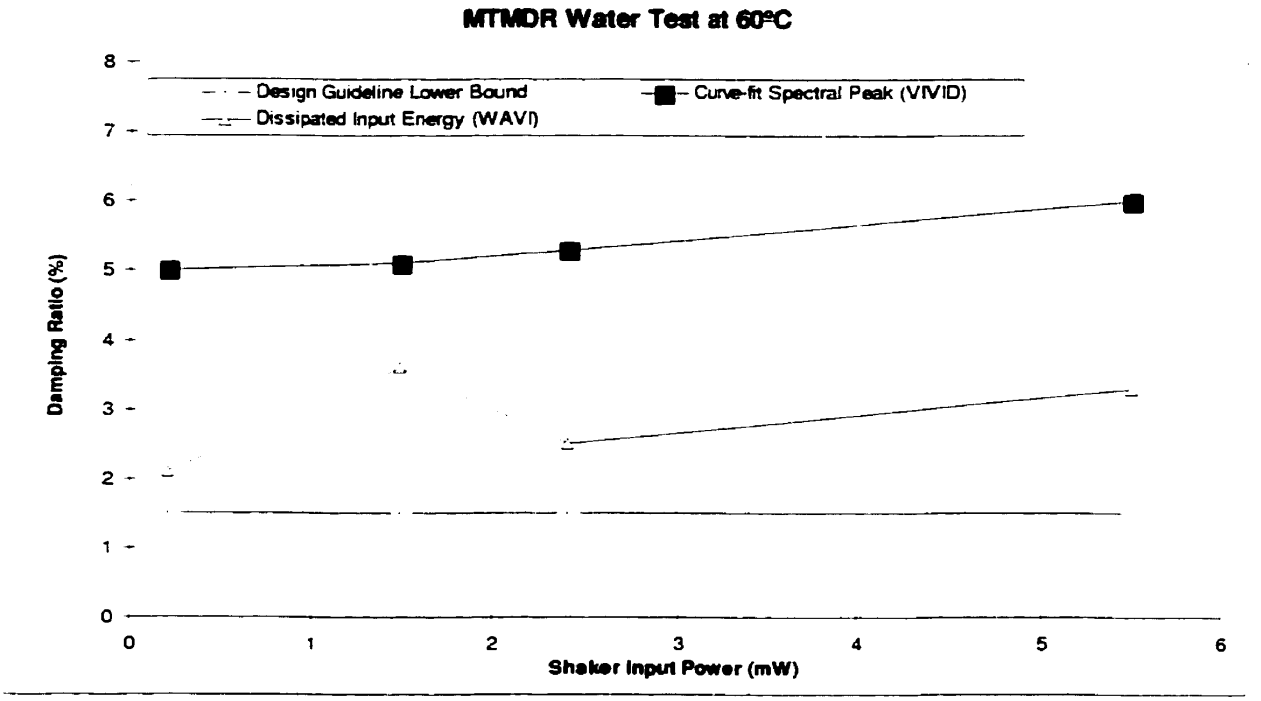

Figure 6.13: MTMDR Water at 60° Test Damping Ratios

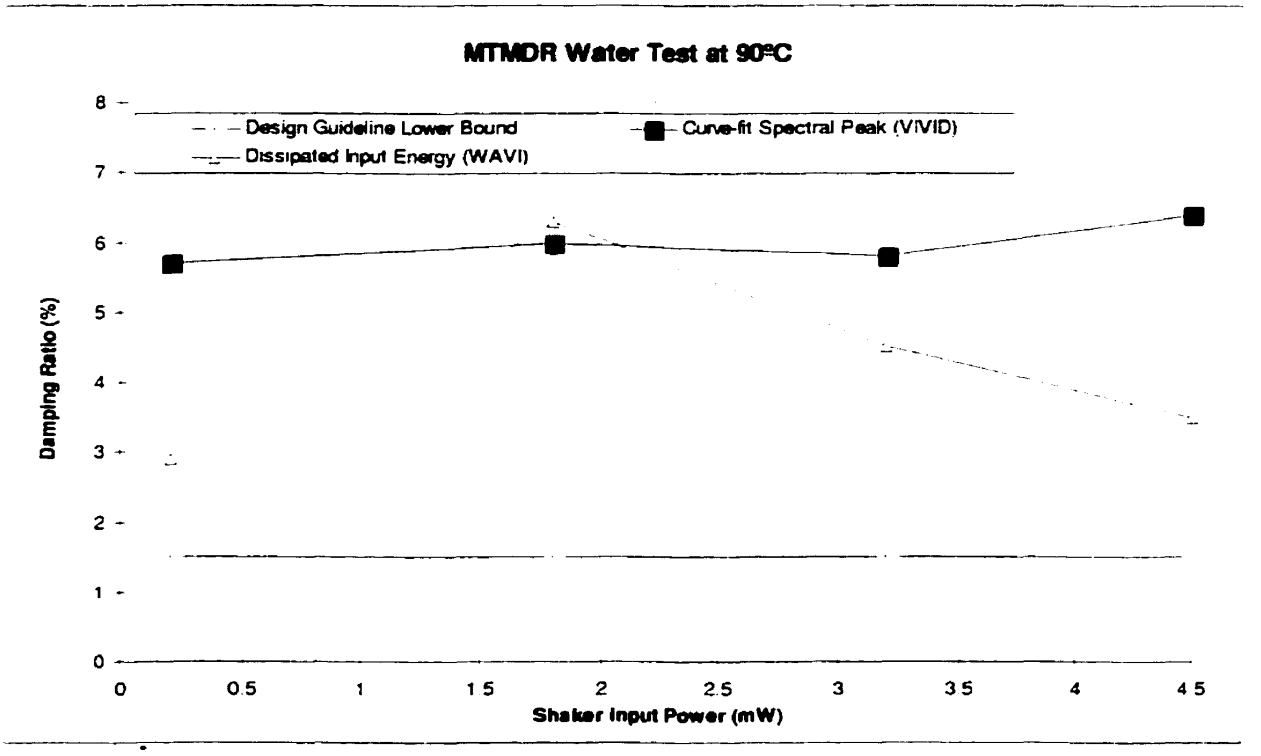

Figure 6.14: MTMDR Water at 90° Test Damping Ratios

6.4 Energy Balances

The shaker power is the energy supplied to the vibrating tube system at a particular rate. The total support work-rate is the rate that the tube system returns energy to the stationary supports. If the system is not storing energy in any way, the support work-rate should be equal to the shaker work-rate minus the rate that energy is lost to other forms of damping.

Figures 6.15 to 6.20 contain graphs comparing input work-rates supplied by the shakers and energy dissipated by damping. Dissipated work-rates are the sum of work-rates measured at the supports with WAVI, and work-rates estimated from the viscous damping.

Shaker work-rates and support (friction) work-rates have already been reported in Tables 5.4 (air) and 5.5 (water) for the RTMDR, and in Tables 5.10 (air) and 5.11 (water) for the MTMDR. Work-rates dissipated by viscous damping in water tests have been calculated using the formulae of Chapter 2. These work-rate estimates are added to the measured support work-rate for a total dissipated work-rate. The following graphs compare those dissipated values with the total input work-rate measured from the shakers.

Work-rates due to squeeze-film damping were not added to the dissipation work-rates due to viscous and friction damping. No theoretical formula exists for squeeze-film damping (Pettigrew et al.'s relation is only an empirical bound). In addition, it is expected that some of the squeeze-film forces will be transferred to the force transducers in the support. Any motion that is not purely radial may produce forces that are included in support work-rates.

For example, Table 5.5 lists the first RTMDR water test shaker work-rate as 1.9 mW and the support (friction) work-rate as 1.1 mW. The viscous damping is (Subsection 5.1.5) 0.36%. The work dissipated per cycle (Equation 2.7) is

$$W_d = 8\pi^3 m\zeta {f_n}^2 X^2$$

$$W_d = 8\pi^3(1.374)(0.0036)24^2(92 \times 10^{-6})^2 \approx 6.0 \times 10^{-6}\,\text{J/cycle}$$

which, at a frequency of 24 Hz, corresponds to 0.1 mW. Adding this to the support work-rate results in a total dissipated work-rate of 1.2 mW. Similar calculations are made for all other water tests for both rigs.

The sum of the support work-rates is very close to the shaker power for air tests. This is expected for air tests since the only significant contribution to the damping is friction. It is also expected that the input-output differences are greater for the water tests. Viscous and squeeze-film damping would add to the total damping for a tube vibrating in water.

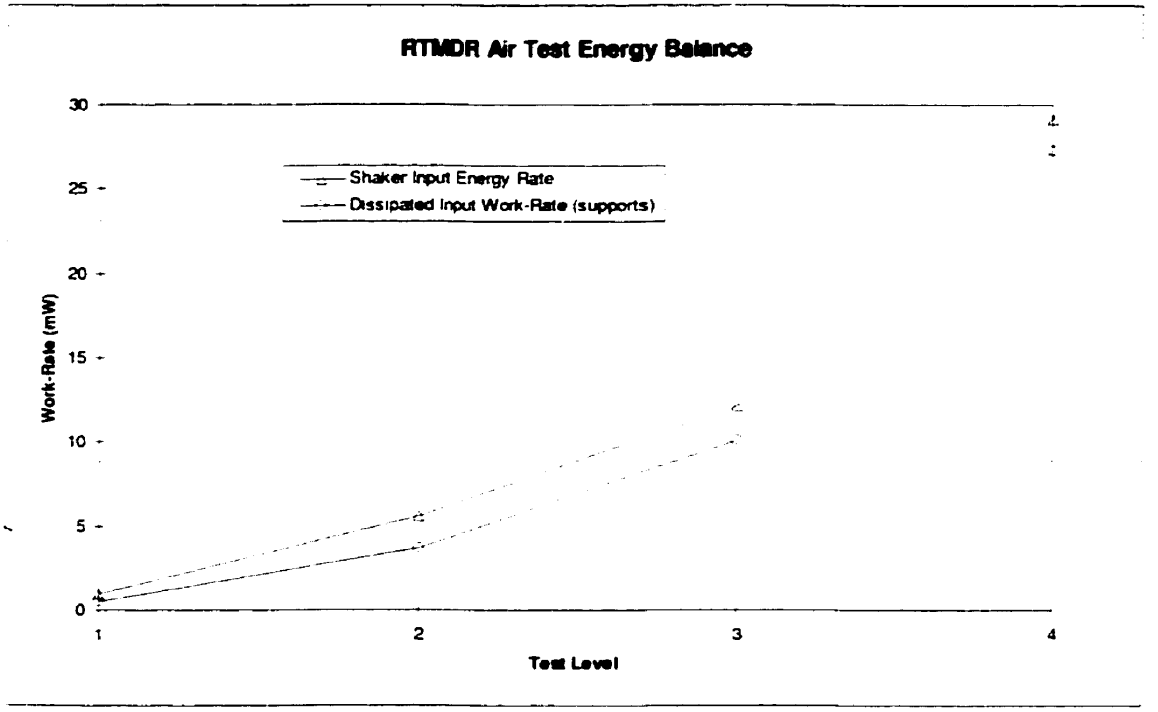

Figure 6.15: RTMDR Air Test Energy Balance

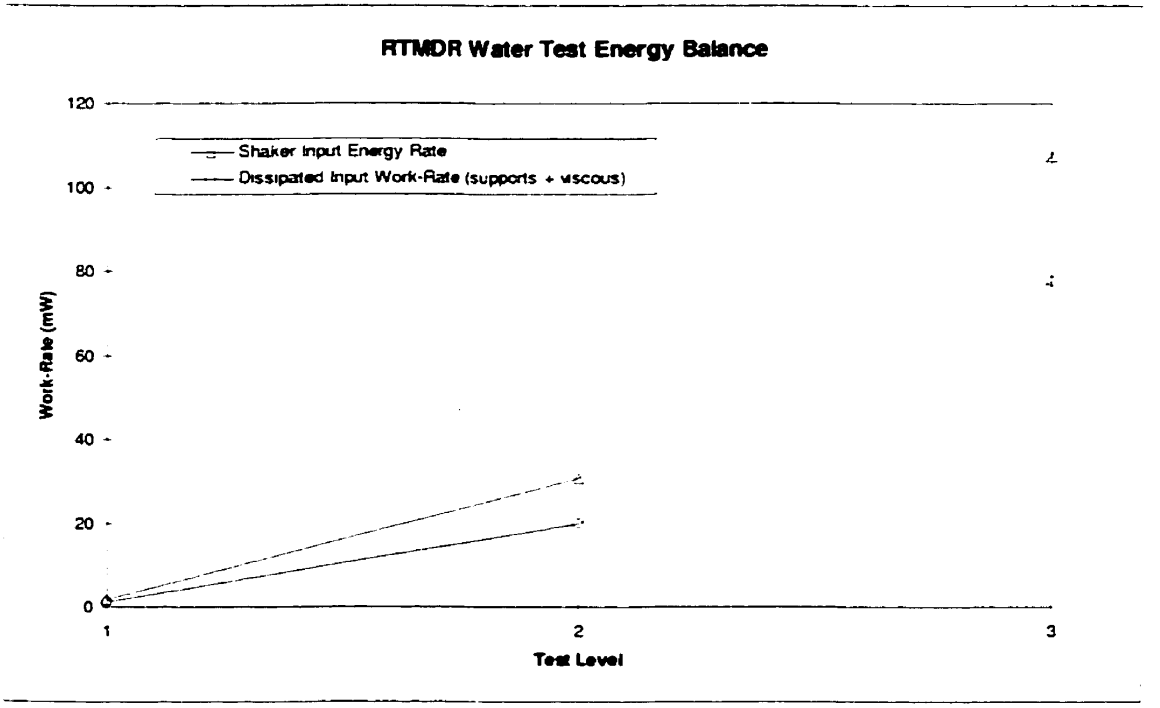

Figure 6.16: RTMDR Water Test Energy Balance

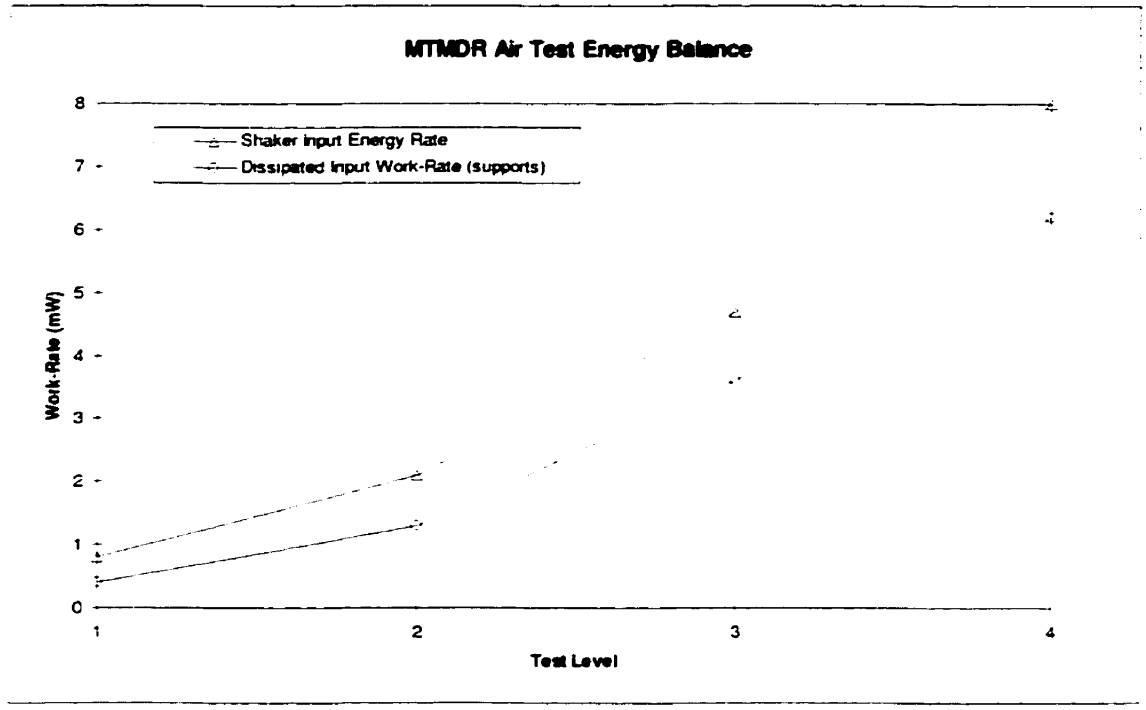

Figure 6.17: MTMDR Air Test Energy Balance

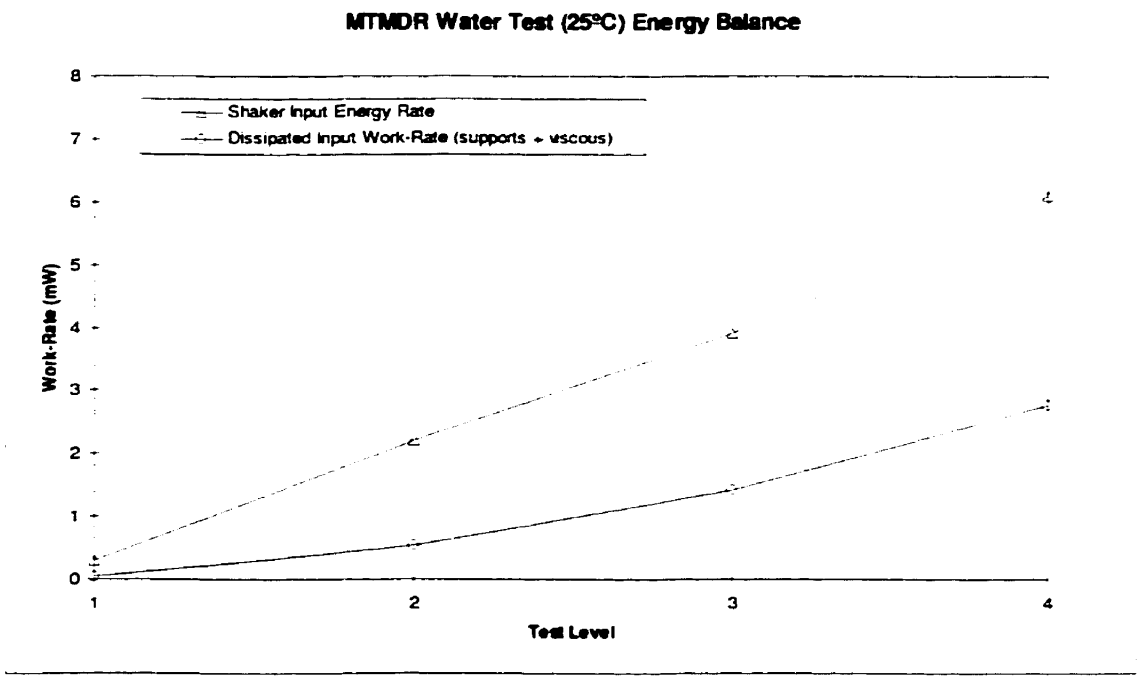

Figure 6.18: MTMDR Water Test (25° C) Energy Balance

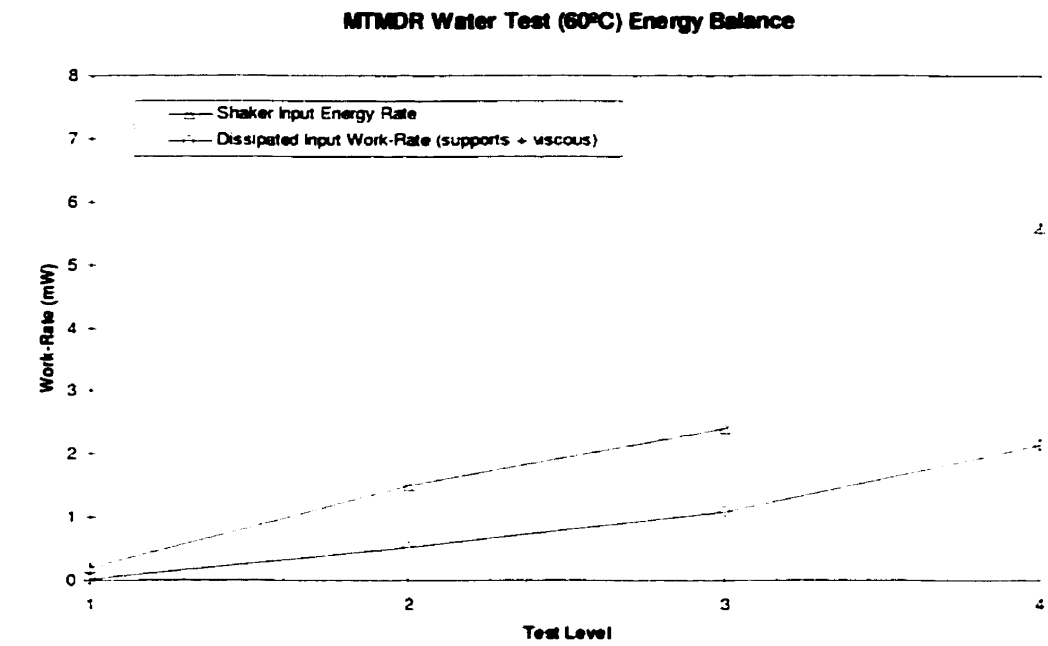

Figure 6.19: MTMDR Water Test (60° C) Energy Balance

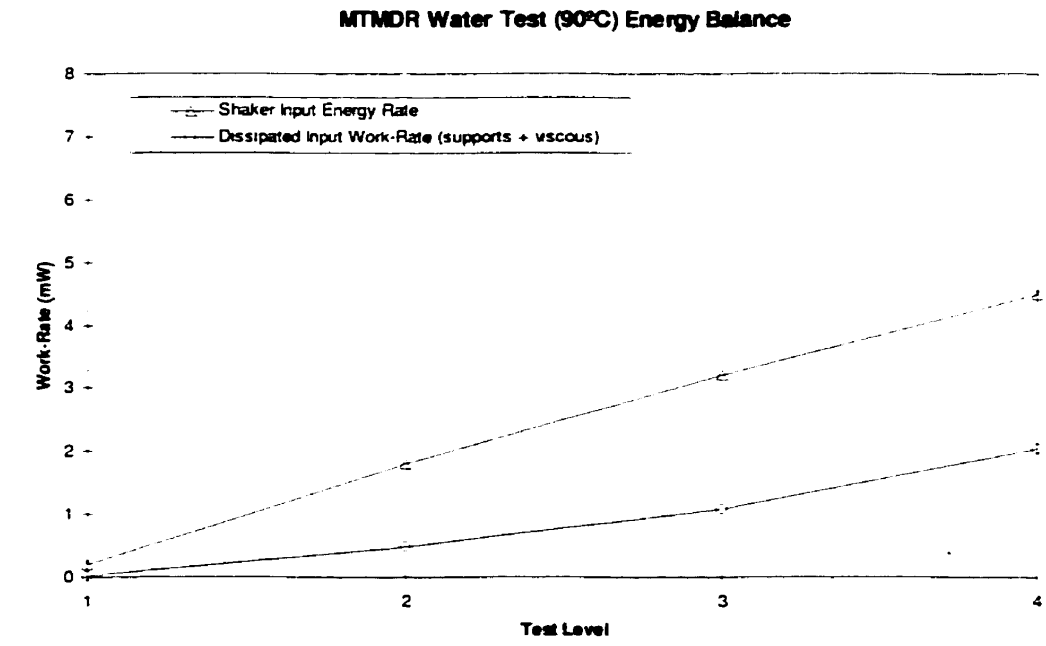

Figure 6.20: MTMDR Water Test (90° C) Energy Balance

Chapter 7

Conclusions

This thesis describes work done to understand damping in multispan heat exchanger tubes.

A test facility was developed to measure damping of multispan heat exchanger tubes in air and in water at different temperatures up to 90°C. This rig is now used for further damping studies.

A computer program named VIVID was developed and used to measure frequency response and tube vibration amplitudes. It can also calculate system parameters such as natural frequency and damping from curve fits of the frequency response. This software has a simple user interface, allows several channels of data to be analyzed simultaneously, and contains advanced numerical routines to allow curve-fitting of two adjacent spectral peaks. VIVID is now used for other applications.

A computer program named WAVI was developed and used to calculate shaker excitation work-rates dissipated at rig supports. WAVI is a development of a program used to measure work-rates in fretting-wear testing. Changes were made to improve the user interface, and to include measurements of shaker work-rates. WAVI was essential to this work, since an important objective was to develop a method of estimating damping using work-rates.

As expected, damping values estimated from the rate of dissipated input energy are slightly greater than the lower limit values of Pettigrew et al.'s guidelines. They are less than values estimated from curve-fitting response spectra. This was expected, since the energy method avoids some of the limitations of the spectral peak method. This energy method appears to be a better method of measuring damping for systems with non-linearities and multi-peak frequency responses, such as heat exchanger tubes.

For the air tests—where friction damping at the support is the only significant damping occurring—the support work-rate is only slightly less than the shaker work-rate, indicating a reasonable energy balance. For water tests, the difference between the support work-rate and shaker work-rate is greater, as expected, due to the additional viscous damping. When the viscous work-rate is added there is still a difference between dissipated work-rate and shaker input work-rate: this may be due to the inability to accurately measure or calculate the squeeze-film energy dissipation. This is the first known time that energy balance and the dissipated energy approach is used to characterize damping of heat exchanger tubes. As mentioned earlier, subsequent work has confirmed the validity of the energy approach.

Damping values did not change significantly with temperature or excitation level. Both of these results agree with past experimental data bounded by Pettigrew et al.'s guidelines, although further work needs to be done to determine why no temperature effect exists.

References

[1] T.M. Mulcahy, "Fluid Forces on Rods Vibrating in Finite Length Annular Regions," ASME Journal of Applied Mechanics, Vol. 47, June 1980, pp. 234–240.

[2] R.J. Rogers, C.E. Taylor, and M.J. Pettigrew, "Fluid Effects on Multi-Span Heat-Exchanger Tube Vibration," Topics in Fluid Structure Interaction, 1984 PVP Conference and Exhibition, San Antonio, Texas, June 1984, pp. 17–26.

[3] J.F. Booker, "Dynamically Loaded Journal Bearings: Mobility Method of Solution," Journal of Basic Engineering, September 1965, pp. 291–300.

[4] M.J. Pettigrew, R.J. Rogers, and C.E. Taylor, "Damping of Heat Exchanger Tubes," AECL Research Report CRNL-3008. Proprietary.

[5] M.J. Pettigrew, H.G.D. Goyder, Z.L. Qiao, and F. Axisa. "Damping of Multispan Heat Exchanger Tubes—Part 1: In Gases," Symposium on Special Topics of Structural Vibration, ASME Pressure Vessels and Piping Conference, Chicago, 1986.

[6] M.J. Pettigrew, R.J. Rogers, and F. Axisa. "Damping of Multispan Heat Exchanger Tubes—Part 2: In Liquids," Symposium on Special Topics of Structural Vibration, ASME Pressure Vessels and Piping Conference, Chicago, 1986.

[7] T. Pike and C.E. Taylor. Personal communication, Chalk River Labs, Atomic Energy of Canada Limited, 1994.

[8] S.S. Chen, M.W. Wambsganss, and J.A. Jendrzejczyk. "Added Mass and Damping of a Vibrating Rod in Confined Viscous Fluids," ASME Journal of Applied Mechanics, Vol. 43, pp. 325–329, 1976.

[9] J. Mastorakos. "A Numerical Technique for Deducing the Dynamic Parameters from Amplitude spectrum Functions," Technical Memorandum SP-VIBR-73, Chalk River Nuclear Laboratories, May 1984.

[10] D.W. Marquardt. "An Algorithm for Least-Squares Estimation of Nonlinear Parameters," Journal Society Industrial Applied Mathematics, Vol. 11, No. 2, June 1963, pp. 431-441.

[11] W. Press, B. Flannery, S. Teukolsky, and W. Vetterling. "Numerical Recipies," Cambridge University Press, 1989.

[12] N.J. Fisher, A.B. Chow, and M.K. Weckwerth. "Experimental Fretting-Wear Studies of Steam Generator Materials," ASME PVP-Vol.273, Flow-Induced Vibration, pp. 241–255, 1994.

[13] W.T. Thomson, "Theory of Vibration with Applications, 3rd ed.," Prentice Hall, 1988, pp. 61–71, 74–75.

[14] C.E. Taylor, M.J. Pettigrew, T.J. Dickinson, I.G. Currie, P. Vidalou, "Vibration Damping in Multispan Heat Exchanger Tubes," ASME Journal of Pressure Vessel Technology, 1998, 120 (3), pp. 283–289.

[15] M.J. Pettigrew, C.E. Taylor, N.J. Fisher, M. Yetisir, B.A.W. Smith, "Flow-Induced Vibration: Recent Findings and Open Questions," Nuclear Engineering and Design, 1998, 185, pp. 249–276.

[16] M. Yetisir, E. McKerrow, M.J. Pettigrew, "Fretting-wear Damage of Heat Exchanger Tubes: A Proposed Damage Criterion Based on Tube Vibration Response," ASME Journal of Pressure Vessel Technology, 1998, 120 (3), pp. 297–305.

[17] I.H. Shames, "Mechanics of Fluids, 2nd ed.," McGraw-Hill, 1982, p. B-36.

Appendix A

LabVIEW and Data Acquisition Parameters

This appendix briefly describes LabVIEW and the data acquisition hardware used for measurements.

VTU is using software developed with LabVIEW because of the program's versatility, portability, and customizable graphical user interfaces. It was logical to use LabVIEW to create specialized tools for the measurements and calculations this work required.

A.1 LabVIEW

LabVIEW for Windows Version 3.0.1[1] runs under Microsoft Windows 3.1 in 386 enhanced mode. It requires a math co-processor, and a minimum 80386-based PC.

LabVIEW requires 2.2 MB of RAM and allocates 4 MB of system memory by default, in addition to memory requirements for Windows and any installed drivers. Experience indicated that vibration frequency analysis generally required more memory, particularly for long averaging periods with many input channels. Analysis for this work was done on

[1] This was the current version of LabVIEW at the time of this work.

a computer with 20 MB of RAM, often with virtual memory assignments up to 40 MB total, so that performance was not compromised.

A.2 Data Acquisition Board

The National Instruments AT-MIO-16-L9 is a high-accuracy, software-configurable 12-bit data acquisition and control plug-in board. The DAQ specifications of this board are shown in the remaining tables of this appendix.

Table A.1: Analog Input Characteristics

Number of channels	16 single-ended or 8 differential
Type of A/D conversion	Sampling, successive approximation
Resolution	12 bits, 1 in 4096
Maximum sampling rate	100,000 samples per second
Input coupling	DC

Table A.2: Input Signal Ranges

Board gain	Board range (V)	Precision (μV)	Maximum multichannel sample rate (kHz)
1	$\pm$10	4880	100
10	$\pm$1	488	100
100	$\pm$0.1	48.8	70
500	$\pm$0.02	9.76	20

The Least Significant Bit (LSB) is the rightmost (and smallest-valued) bit in an A/D sample.

Table A.3: Transfer Characteristics

Relative accuracy	±0.9 LSB typical, ±1.5 LSB max.
Gain error (relative to calibration ref.)	0.0244% of reading max.

Table A.4: Amplifier Characteristics

Input impedance	1 GΩ in parallel with 50 pF

Table A.5: Amplifier Common-Mode Rejection Ratio

Board gain	CMRR, DC to 100 Hz (dB)
1	75
10	95
≤100	105

The Common-Mode Rejection Ratio (CMRR) is a measure (in dB) of an instrument's ability to reject interference from a common-mode signal.

Table A.6: Dynamic Characteristics

Bandwidth (small signal, -3 dB)	650 kHz at gain = 1
Slew rate	5.0 V/μs

Table A.7: Dynamic System Noise

Board gain	$\pm$10 V range
$\leq$10	0.10 LSB RMS
100	0.15 LSB RMS
500	0.30 LSB RMS

Appendix B

VIVID

This appendix describes how VTU previously measured natural frequencies and damping ratios from time-domain data. It also describes how the same information can be determined using VIVID.

B.1 Previous Procedure

The method previously used to measure two-peak damping ratios in VTU was complicated. The procedure is outlined below:

1. Acquire the data and perform a spectral analysis with WAVEPAK (spectral analysis software on a dedicated portable computer).
2. Estimate the six parameters from a graph of the frequency spectrum.
3. Save the spectrum data as a special text file.
4. Edit the text file so that only the frequency and amplitude data pairs for the spectrum remain. The text file contains other data such as parameter inputs and time-domain input.
5. Create a text file with estimates of the six parameters from Step 2.

6. Run the VTU program 2PEAK. Supply the spectrum data file name, the frequency range for the curve fit, and the parameter estimate file name. 2PEAK iterates and displays its final solution for parameters. If a solution is not reached (i.e., divergence) make new parameter estimates and repeat Steps 5 and 6.

This method required transferring data between at least three programs (WAVEPAK, a text editor, and 2PEAK). A user may have to graph the data to get an idea of suitable initial guesses before running 2PEAK. In addition, only two data channels can be acquired by WAVEPAK at once. Repeated acquisitions and analyses are necessary if the experiment recorded more than two channels of data.

B.2 New Procedure

The procedure developed to calculate damping ratios for this work is simpler. The procedure is a subroutine of a larger LabVIEW analysis program (VIVID).

1. Acquire the data and perform a spectral analysis with VIVID.

2. Select a channel. LabVIEW shows a new screen with a plot of the selected spectra.

3. Select one- or two-peak fitting.

4. Move graph cursors to delimit a spectral peak.

5. A dialog box appears in the top left corner of the screen and prompts the user to supply initial guesses.

6. Program iterates and displays its final solutions for the parameters. It also overlays the best-fit plot over the spectral data points. The user can print this display. Finally, control reverts back to the analysis VI. The user can then do damping ratio curve fits of the other channels or acquire new data.

The method is both simpler and more versatile. The user does not have to switch between platforms and the VIs guide one through the steps with prompts and messages. The number of data channels that can be analyzed simultaneously is greater than was possible with WAVEPAK. The analyses done for this work were accomplished using a data acquisition board with 16 analog input channels and a maximum total acquisition rate of 100 kHz (e.g., 10 channels at 10 kHz each, maximum).

The structure of the damping ratio subroutine is shown below. A description of its function follows.

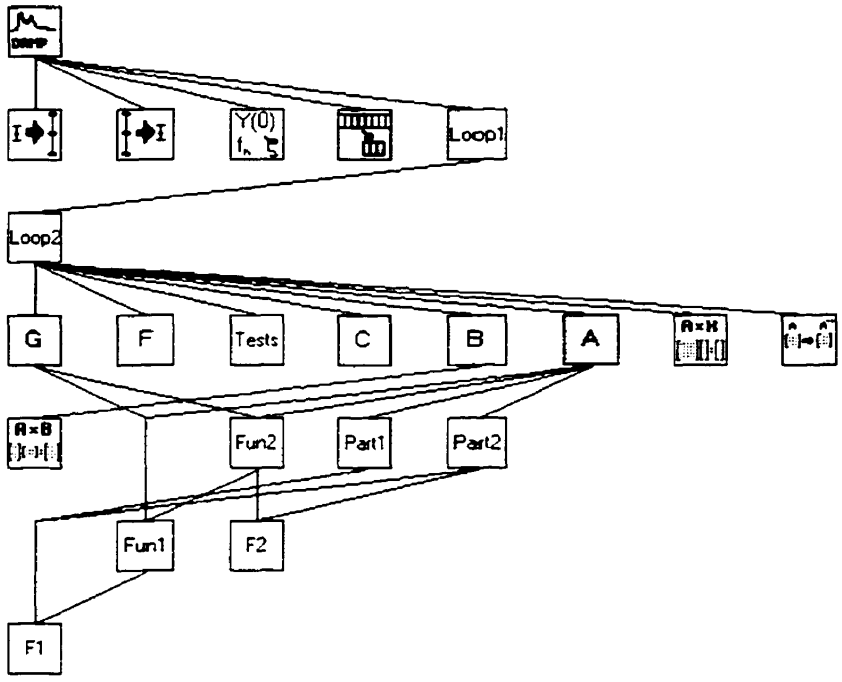

Figure B.1: Damping ratio substructure hierarchy of VIVID

When a user presses the appropriate *Damping* front panel button, the spectrum for the currently-selected channel is passed to subVI DAMP. This subVI sends the information to its own subVIs to do the iterative curve fit and return the damping ratio parameter.

When called, a subVI named DAMP displays its front panel with three fields:

1. *Input* has a control for the user to select one or two peaks, a control to set the maximum number of iterations to calculate, and buttons that will perform the

curve fit or return to the VIVID top-level VI.

2. *Notes* displays the date and time, the channel number analyzed, sample duration and number of averages, and analysis frequency resolution. There is also a box where the user can enter additional information if desired.

3. *Output* has displays that indicate the parameters calculated after each iteration and the current iteration number. It also has a graph that shows a plot of the acquired frequency spectrum data points. When the iteration is done, it overlays this information with a line plot of the calculated fit.

After the user sets the controls in *Input* and presses the button to perform the fit, the following procedure executes in DAMP:

1. The date and time, the channel number, and sample data that were passed to DAMP are displayed. The spectral data is re-plotted.

2. The program is paused. This allows the user to position cursors to delimit the spectral peak (or peaks) they wish to fit.

3. When the *Fit* button is pressed, SELECT INRANGE is called to remove the part of the spectrum the user delimited. DAMP SCALE scales that selection into a range from 0 to 10^{-5}. The iterative method works more reliably when the values are scaled within this range. Scaled amplitudes and the corresponding frequency values are passed to subVI LOOP1.

4. SubVI GUESSES is called and the user is prompted for initial parameter values. The user prompt appears in a small window in the upper left-hand corner of the screen so that the user can still see the spectral plot data underneath. If there is only one peak to be fit then there are three required inputs. If there are two peaks then six parameters are required. Note that the default values for the zero-frequency amplitude and damping ratio (0.00001 and 0.001, respectively) are nearly always

adequate for the curve-fitting iteration. Users should attempt to make an accurate guess at the peak natural frequency, however. The equations involved make the Marquardt method's convergence very sensitive to this parameter. These guesses are returned to LOOP1.

5. The number of iteration parameters and convergence criteria are passed to LOOP2.

6. LOOP2 performs the calculations necessary for the Marquardt iteration method.

7. LOOP1 executes in a *While Loop*. It stops when its convergence criteria are met (i.e., it finds a solution) or when the iteration number exceeds the iteration limit set by the user. The calculated parameters are scaled back to their correct values by a call to DAMP SCALE BACK and displayed on the front panel after each iteration.

8. After the *While Loop* finishes, DAMP calculates a plot for the frequency range that the user selected using the final values of the parameters it has calculated. This plot is then superimposed on the spectral data.

9. The user may then repeat the process (with new initial guesses, for instance, if the method did not converge) or stop the damping ratio subroutine and return to the VIVID program.

Appendix C

WAVI

Work-rate Analysis Virtual Instrument (WAVI) is a computer program that runs under LabVIEW.

From the user interface the user sets acquisition and analysis parameters, starts the program, and views results. WAVI calls other subVIs in the sequence required to calculate work-rates.

Data is acquired from tape. WAVI acquires four channels of data (two displacement signals and two force signals) at the acquisition speed and for the duration set by the user. It then converts the forces from Cartesian coordinates to cylindrical coordinates, adds the displacement *transducer angle* set by the user (see Figure C.1), and converts back to rectangular co-ordinates. Transducer angle indicates the angle between the orthogonal displacement measurements and the orthogonal force measurements. The transducer angle for these tests was -45°.

WAVI calculates the resultant of the two forces, plots the array on a graph, and displays the result for the user. The user may set a minimum force level at this stage. If a force level is set then every signal point below that level is assigned a zero (0) and every point above that level is assigned a value of one (1). This is the *contact array.* The product of the contact array and the resultant force is the *masked force.* The masked

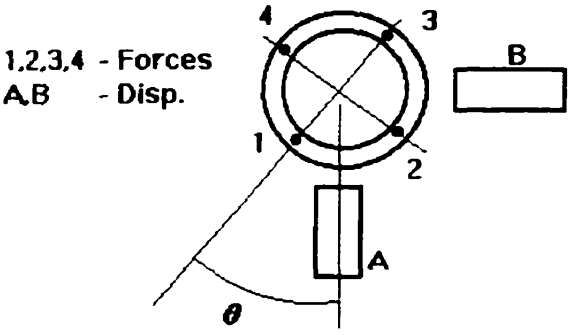

Figure C.1: Force and Displacement Transducer Layout

force is displayed for the user as well. All elements in the contact array are summed and the result is divided by the size of the array and multiplied by 100%. This is the *time* the tube spends in contact with the support as a percentage of the total sample duration.

WAVI then resolves the impact forces into *normal* and *shear* components at the point of contact and calculates force statistics (mean, maximum and RMS). It then takes the displacement and contact arrays and calculates sliding distance, total displacement and RMS displacements. It does this by calculating $x_i - x_{i-1}$ and $y_i - y_{i-1}$ for $i = 1$ to $N - 1$, producing an array of displacement differences, $[X]$ and $[Y]$. These arrays of differences are each summed for the *total displacements.*

The arrays of differences are multiplied by the contact array. This removes any values where there is no contact. The sum of these resultant differences is the sum of displacements that occur during contact and is the *sliding distance.* Normal, shear, and resultant force arrays are multiplied by the contact array for a *masked force array.*

These masked force and X and Y arrays are used to calculate normal, shear, and total work-rates. The average force between two successive force values in the signal arrays is

$$F_{av,i} = 0.5\,(F_{i+1} + F_i)$$

Using the arrays of displacement differences

$$\Delta W_i = F_{av,i}\left(\sqrt{\Delta X_i^2 + \Delta Y_i^2}\right)$$

Note that this equation is true for each of what the program calls "normal" and "shear" work-rates. *Normal* work is defined as the normal force of the tube-support contact multiplied by the sliding distance travelled. *Shear* work is defined as the sliding force multiplied by the sliding distance traveled. Not that normal work is not "work," in the strict physical sense since the incremental forces and displacements are orthogonal. Normal work-rate is a quantity that has traditionally been used to predict fretting-wear tube damage.

WAVI uses the total displacement, not just the sliding component, to calculate work-rate. However, non-contacting motions will be multiplied by zero force values since the work-rate is calculated by multiplying the user-defined contact array forces with the displacements. This procedure might produce errors if motions are very small and radial motion is of the magnitude of sliding motion.

Another possible source of error to these work-rate calculations might occur when the tube is impacting[1] the support. A significant squeeze-film force may be generated when the tube approaches the support, and the tube will do work on the fluid if it continues to move against this force. However, if the tube is impacting (a purely radial motion) there will be no circumferential component to its displacement and no work will be measured for this motion, even if the force falls above the cutoff threshold. This means that the actual work-rate of a tube at a support in a liquid may be higher than that calculated according to the definition given above.

The total work is calculated by

$$W = \sum \Delta W_i$$

The total work divided by the sample duration is the *work-rate.*

When the calculations are done, the computer emits a beep to notify the user. All results are displayed on screen, and may be printed out in a summary report.

[1] See Figure 2.1.